

$D^{(*)}\bar{B}^{(*)}$ Dynamics in Chiral Effective Field Theory

Zhe Liu^{1,2,5,*}, Hao Xu^{4,†} and Xiang Liu^{1,2,3,5,‡}

¹*School of Physical Science and Technology, Lanzhou University, Lanzhou 730000, China*

²*Lanzhou Center for Theoretical Physics, Key Laboratory of Theoretical Physics of Gansu Province, Key Laboratory of Quantum Theory and Applications of MoE,*

Gansu Provincial Research Center for Basic Disciplines of Quantum Physics, Lanzhou University, Lanzhou 730000, China

³*MoE Frontiers Science Center for Rare Isotopes, Lanzhou University, Lanzhou 730000, China*

⁴*Institute of Theoretical Physics, College of Physics and Electronic Engineering, Northwest Normal University, Lanzhou 730070, China*

⁵*Research Center for Hadron and CSR Physics, Lanzhou University and Institute of Modern Physics of CAS, Lanzhou 730000, China*

(Dated: March 14, 2025)

In this work, we systematically study the interactions of the S -wave $D^{(*)}\bar{B}^{(*)}$ systems within the framework of chiral effective field theory in heavy hadron formalism. We calculate the $D^{(*)}\bar{B}^{(*)}$ effective potentials up to next-to-leading order, explore the bound state formations, and investigate the $D^{(*)}\bar{B}^{(*)}$ scattering properties such as scattering rate, scattering length, and effective range. Our results show that all $I = 1$ $D^{(*)}\bar{B}^{(*)}$ potentials are repulsive, preventing the formation of bound states, while the $I = 0$ potentials are generally attractive. Specifically, we get two important observations: first, the shallow bound state is more likely to exist in the $D\bar{B}[I(J^P) = 0(0^+)]$ system than in the $D\bar{B}^*[I(J^P) = 0(1^+)]$ system; second, $D^*\bar{B}^*[I(J^P) = 0(0^+)]$ and $D^*\bar{B}^*[I(J^P) = 0(1^+)]$ systems possess relatively large binding energies and positive scattering lengths, which suggests strong bound state formations in these channels. So the attractions in the $D^*\bar{B}^*[I = 0]$ systems are deeper than those in the $D\bar{B}^{(*)}[I = 0]$ systems, thus we strongly recommend the future experiment to search for the $D^*\bar{B}^*[I = 0]$ tetraquark systems. In addition, we also investigate the dependencies of the $D\bar{B}^{(*)}$ binding energies on the contact low-energy coupling constants (LECs).

I. INTRODUCTION

The study of exotic hadrons has become a vibrant frontier in particle physics, offering profound insights into the nonperturbative regime of strong interaction. In recent years, the LHCb Collaboration has made groundbreaking discoveries that have significantly advanced our understanding of multi-quark states. In 2020, LHCb reported the observation of two resonances, $X_0(2900)$ and $X_1(2900)$, in the D^-K^+ invariant mass spectrum of the $B^+ \rightarrow D^+D^-K^+$ decay process [1, 2]. These states, with quantum numbers $J^P = 0^+$ and $J^P = 1^+$, respectively, were identified as the first tetraquark candidates with the exotic quark content $ud\bar{s}\bar{c}$. This discovery was followed in 2021 by the observation of the double-charm tetraquark state T_{cc}^+ in the $D^0D^0\pi^+$ invariant mass spectrum [3, 4]. Shortly thereafter, LHCb reported two additional open heavy-flavor tetraquark candidates, $T_{cs0}^a(2900)^{++}$ and $T_{cs0}^a(2900)^0$, in the $D_s^+\pi^\pm$ final states of the $B^+ \rightarrow D^-D_s^+\pi^+$ and $B^0 \rightarrow \bar{D}^0D_s^+\pi^+$ decays [5, 6]. These states are believed to have the quark content $c\bar{s}ud$.

These experimental discoveries have spurred extensive theoretical investigations into the nature of open heavy-flavor multi-quark states. Various approaches, including QCD sum rules, lattice QCD, and effective field theories, have been employed to explore their properties and

structures (see Refs. [7–33] for comprehensive reviews). These studies have deepened our understanding of the exotic hadron spectrum and highlighted the importance of investigating the interactions of dimeson systems, particularly those involving doubly heavy quarks.

Doubly heavy dimeson systems have attracted significant theoretical interest due to their potential to form stable or quasi-stable molecular states. For instance, Li *et al.* explored the possibility of deuteron-like molecular states in $D^{(*)}D^{(*)}$, $\bar{B}^{(*)}\bar{B}^{(*)}$, and $D^{(*)}\bar{B}^{(*)}$ systems, identifying several promising candidates [34]. QCD sum rules have been applied to study exotic open-flavor tetraquark states such as $bc\bar{q}\bar{q}$, $bc\bar{s}\bar{s}$, $qc\bar{q}\bar{b}$, and $sc\bar{s}\bar{b}$, revealing that some of these states lie below the $D^{(*)}B^{(*)}$ and $D_s^{(*)}B_s^{(*)}$ thresholds, making them susceptible to decay via fall-apart mechanisms [35]. The color-magnetic interaction model has also been used to calculate mass splittings for $qq\bar{Q}\bar{Q}$ tetraquark states [36], while the molecular picture has been employed to investigate the binding energies of T_{cc}^+ and its bottom and strange partners [37]. Additionally, the complex scaling method (CSM) has been utilized to study doubly heavy tetraquark bound and resonant states [38].

The stability of doubly heavy tetraquarks, particularly those involving bottom and charm quarks, remains a topic of active debate. While some studies suggest that states such as $bb\bar{u}\bar{d}$, $bb\bar{u}\bar{s}$, and $bb\bar{d}\bar{s}$ are stable against strong decay [39], others argue that bottom-charm tetraquarks may not be stable [40–46]. The production mechanisms and detection prospects for these states at colliders have also been explored, with esti-

* zhliu20@lzu.edu.cn

† xuh2020@nwnu.edu.cn

‡ xiangliu@lzu.edu.cn

mates suggesting significant production cross sections for double-bottom and mixed bottom-charm tetraquarks at the LHC [47].

Recent lattice QCD studies have provided further insights into the properties of doubly heavy tetraquarks. Meinel *et al.* found no evidence for QCD-stable $\bar{b}cud$ tetraquark states [48], while Alexandrou *et al.* and Padmanath *et al.* reported shallow bound states for isoscalar $\bar{b}cud$ systems [49, 50]. These findings, along with the identification of sub-threshold poles in the $D\bar{B}$ scattering amplitude [51], significantly advanced our understanding of the weak decay behaviors of $D\bar{B}$ molecules [52].

In this work, we investigate the interactions of S -wave $D\bar{B}$, $D\bar{B}^*$, and $D^*\bar{B}^*$ systems using chiral effective field theory (ChEFT) in the heavy hadron formalism. ChEFT, a low-energy effective theory of QCD, has proven to be a powerful tool for studying hadronic interactions, particularly in the context of nucleon-nucleon systems [53, 54]. By incorporating heavy-quark and chiral symmetries, ChEFT provides a robust framework for analyzing the interactions of heavy mesons. Previous studies have applied ChEFT to systems such as $D^{(*)}D^{(*)}$ [55, 56], $\bar{B}^{(*)}\bar{B}^{(*)}$ [57], and hidden-charm systems [58], as well as to the interactions of heavy pentaquark molecular states [59–61]. These investigations have demonstrated the effectiveness of ChEFT in describing the low-energy dynamics of heavy hadrons.

This paper is organized as follows: In Sec. II, we introduce the chiral effective Lagrangians with $SU(2)$ flavor symmetry used in our calculations. In Sec. III, we present the scattering amplitudes and derive the effective meson-meson potentials. In Sec. IV, we analyze the numerical results, examining the behaviors of the effective potentials and searching for possible bound states by solving the Schrödinger equation. We also discuss the scattering T -matrix and extract physical quantities such as the scattering rate, scattering length, and effective range. Finally, in Sec. V, we summarize our findings and discuss their implications for future studies of doubly heavy tetraquark systems.

II. EFFECTIVE LAGRANGIANS

Within the framework of ChEFT in the heavy hadron formalism, the low-energy $D^{(*)}\bar{B}^{(*)}$ scattering amplitudes are expanded order by order in terms of a small parameter $\epsilon = q/\Lambda_\chi$, where q represents the momentum of a Goldstone boson, the mass difference between D^* and D mesons (or \bar{B}^* and \bar{B} mesons), or the residual momentum of a heavy meson. The parameter Λ_χ denotes the chiral symmetry broken scale or the mass of

the heavy mesons.

A. Lagrangians at the leading order

At leading order (LO), the Lagrangian describing the LO contact $D^{(*)}\bar{B}^{(*)}$ interaction is:

$$\begin{aligned} \mathcal{L}_{4H}^{(0)} = & D_a \text{Tr}[H\gamma_\mu \bar{H}] \text{Tr}[H\gamma^\mu \bar{H}] \\ & + D_b \text{Tr}[H\gamma_\mu \gamma_5 \bar{H}] \text{Tr}[H\gamma^\mu \gamma_5 \bar{H}] \\ & + E_a \text{Tr}[H\gamma_\mu \tau^a \bar{H}] \text{Tr}[H\gamma^\mu \tau_a \bar{H}] \\ & + E_b \text{Tr}[H\gamma_\mu \gamma_5 \tau^a \bar{H}] \text{Tr}[H\gamma^\mu \gamma_5 \tau_a \bar{H}], \end{aligned} \quad (1)$$

where D_a , D_b , E_a , and E_b are independent LECs, τ^α represents the Pauli matrix in isospin space. The heavy meson doublet (D, D^*) or (\bar{B}, \bar{B}^*) is described by the H field in the heavy hadron formalism [55, 57, 58]:

$$\begin{aligned} H &= \frac{1+\not{v}}{2}(P_\mu^* \gamma^\mu + iP\gamma_5), \\ \bar{H} &= \gamma^0 H^\dagger \gamma^0 = (P_\mu^{*\dagger} \gamma^\mu + iP^\dagger \gamma_5) \frac{1+\not{v}}{2}, \\ P &= (D^0, D^+) \quad \text{or} \quad (B^-, \bar{B}^0), \\ P_\mu^* &= (D^{*0}, D^{*+})_\mu \quad \text{or} \quad (B^{*-}, \bar{B}^{*0})_\mu, \end{aligned} \quad (2)$$

where $v = (1, 0, 0, 0)$ is the four-velocity of the heavy mesons. For the $D^*\bar{B}^*$ system, the scattering amplitudes receive contributions from the one-pion exchange interactions at LO. The Lagrangian for the LO $D^*D^*\pi$ vertex or $\bar{B}^*\bar{B}^*\pi$ vertex is given by [55, 57, 58]

$$\begin{aligned} \mathcal{L}_{H\phi}^{(1)} = & -\langle (iv \cdot \partial H) \bar{H} \rangle + \langle H v \cdot \Gamma \bar{H} \rangle + g \langle H \not{v} \gamma_5 \bar{H} \rangle \\ & - \frac{1}{8} \Delta \langle H \sigma^{\mu\nu} \bar{H} \sigma_{\mu\nu} \rangle, \end{aligned} \quad (3)$$

$$\Gamma_\mu = \frac{i}{2} [\xi^\dagger, \partial_\mu \xi], \quad u_\mu = \frac{i}{2} \{\xi^\dagger, \partial_\mu \xi\}, \quad (4)$$

where Δ in the last term represents the mass splitting between D and D^* (or \bar{B} and \bar{B}^*), Γ_μ is the chiral connection, u_μ is the axial vector current, and $\xi = \exp(i\phi/2f)$. f is the bare pion decay constant, and the pion field ϕ is

$$\phi = \begin{pmatrix} \pi^0 & \sqrt{2}\pi^+ \\ \sqrt{2}\pi^- & -\pi^0 \end{pmatrix}. \quad (5)$$

B. Lagrangians at next-to-leading order

At next-to-leading order (NLO), the scattering amplitudes receive contributions from one-loop corrections to the LO contact interaction, one-loop corrections to LO one-pion-exchange (OPE), and the two-pion-exchange (TPE) terms. To renormalize these loop contributions, we employ the contact Lagrangians at NLO as follows:

$$\begin{aligned} \mathcal{L}_{4H}^{(2,h)} = & D_a^h \text{Tr}[H\gamma_\mu \bar{H}] \text{Tr}[H\gamma^\mu \bar{H}] \text{Tr}(\chi_+) + D_b^h \text{Tr}[H\gamma_\mu \gamma_5 \bar{H}] \text{Tr}[H\gamma^\mu \gamma_5 \bar{H}] \text{Tr}(\chi_+) \\ & + E_a^h \text{Tr}[H\gamma_\mu \tau^a \bar{H}] \text{Tr}[H\gamma^\mu \tau_a \bar{H}] \text{Tr}(\chi_+) + E_b^h \text{Tr}[H\gamma_\mu \gamma_5 \tau^a \bar{H}] \text{Tr}[H\gamma^\mu \gamma_5 \tau_a \bar{H}] \text{Tr}(\chi_+), \end{aligned} \quad (6)$$

$$\begin{aligned} \mathcal{L}_{4H}^{(2,v)} = & \{ D_{a1}^v \text{Tr}[(v \cdot DH)\gamma_\mu (v \cdot D\bar{H})] \text{Tr}[H\gamma^\mu \bar{H}] + D_{a2}^v \text{Tr}[(v \cdot DH)\gamma_\mu \bar{H}] \text{Tr}[(v \cdot DH)\gamma^\mu \bar{H}] \\ & + D_{a3}^v \text{Tr}[(v \cdot DH)\gamma_\mu \bar{H}] \text{Tr}[H\gamma^\mu (v \cdot D\bar{H})] + D_{a4}^v \text{Tr}[(v \cdot D)^2 H\gamma_\mu \bar{H}] \text{Tr}[H\gamma^\mu \bar{H}] \\ & + D_{b1}^v \text{Tr}[(v \cdot DH)\gamma_\mu \gamma_5 (v \cdot D\bar{H})] \text{Tr}[H\gamma^\mu \gamma_5 \bar{H}] + \dots \\ & + E_{a1}^v \text{Tr}[(v \cdot DH)\gamma_\mu \tau^a (v \cdot D\bar{H})] \text{Tr}[H\gamma^\mu \tau_a \bar{H}] + \dots \\ & + E_{b1}^v \text{Tr}[(v \cdot DH)\gamma_\mu \gamma_5 \tau^a (v \cdot D\bar{H})] \text{Tr}[H\gamma^\mu \gamma_5 \tau_a \bar{H}] + \dots \} + \text{H.c.}, \end{aligned} \quad (7)$$

$$\begin{aligned} \mathcal{L}_{4H}^{(2,q)} = & \{ D_1^q \text{Tr}[(D^\mu H)\gamma_\mu \gamma_5 (D^\nu \bar{H})] \text{Tr}[H\gamma_\nu \gamma_5 \bar{H}] + D_2^q \text{Tr}[(D^\mu H)\gamma_\mu \gamma_5 \bar{H}] \text{Tr}[(D^\nu H)\gamma_\nu \gamma_5 \bar{H}] \\ & + D_3^q \text{Tr}[(D^\mu H)\gamma_\mu \gamma_5 \bar{H}] \text{Tr}[H\gamma_\nu \gamma_5 (D^\nu \bar{H})] + D_4^q \text{Tr}[(D^\mu D^\nu H)\gamma_\mu \gamma_5 \bar{H}] \text{Tr}[H\gamma_\nu \gamma_5 \bar{H}] \\ & + E_1^q \text{Tr}[(D^\mu H)\gamma_\mu \gamma_5 \tau^a (D^\nu \bar{H})] \text{Tr}[H\gamma_\nu \gamma_5 \tau_a \bar{H}] + \dots \} + \text{H.c.}, \end{aligned} \quad (8)$$

where

$$\tilde{\chi}_\pm = \chi_\pm - \frac{1}{2} \text{Tr}[\chi_\pm], \quad \chi_\pm = \xi^\dagger \chi \xi^\dagger \pm \xi \chi \xi, \quad \chi = m_\pi^2. \quad (9)$$

The low-energy constants appearing in the above equations are split into finite and infinite parts. The infinite parts are used to cancel the divergences of the loop contributions at NLO. The finite parts also contribute to the amplitudes, and they additionally introduce a large number of LECs.

After the scattering amplitudes for the $D^{(*)}\bar{B}^{(*)}$ systems are calculated using the above Lagrangians, the effective potentials in momentum space can be obtained via the relation:

$$\mathcal{V}(q) = -\frac{\mathcal{M}(q)}{4}, \quad (10)$$

where the factor $-1/4$ comes from the Breit approximation. To understand the interactions and further investigate whether the $D^*\bar{B}^{(*)}$ systems can form stable molecular states, we need the potentials in coordinate space. Fourier transformations of the momentum-space potentials allow for their derivation:

$$\mathcal{V}(r) = \int \frac{d^3\mathbf{q}}{(2\pi)^3} \mathcal{V}(\mathbf{q}) e^{-i\mathbf{q}\cdot\mathbf{r}} \mathcal{F}(\mathbf{q}), \quad (11)$$

where $\mathcal{F}(\mathbf{q})$ is a regulator function. To avoid ultraviolet (UV) divergence in the integral, we use a Gaussian regulator function $\mathcal{F}(\mathbf{q}) = \exp(-\mathbf{q}^{2n}/\Lambda^{2n})$ with $n = 2$ [55, 57, 58]. Based on the potentials in coordinate space, we can solve the Schrödinger equations to search for the possible bound states.

Simultaneously, according to the effective potentials in momentum space, we can also solve the Lippmann-Schwinger equations (LSE) to calculate the partial-wave two-body scattering amplitudes T :

$$\begin{aligned} T_l(k, k') = & V_l(k, k') \\ & + \int \frac{q^2 dq}{(2\pi)^3} \mathcal{V}_l(k, q) \mathcal{G}(E, q) T_l(q, k'), \end{aligned} \quad (12)$$

where $E = p^2/(2\mu)$ is the energy and μ is the reduced mass. The Green's function $\mathcal{G}(E, q)$ is given by

$$\mathcal{G}(E, q) = \frac{1}{E - (q^2/2\mu) + i\epsilon}. \quad (13)$$

The relation between the T matrix and the phase shift δ is

$$T_l = e^{i\delta} \sin\delta_l. \quad (14)$$

Considering the S -wave, in the low-energy limit the $k \cot\delta_0(k)$ can be expanded in powers of k^2 :

$$k \cot\delta_0(k) = -\frac{1}{a} + \frac{1}{2} r_0 k^2 + \dots, \quad (15)$$

where a is the scattering length and r_0 is the effective range. The ellipsis represents higher-order terms in k . The S -wave scattering cross-section is proportional to the phase shift:

$$\sigma_0(k) = \frac{4\pi}{k^2} \sin^2\delta_0(k). \quad (16)$$

To facilitate a comparison with lattice QCD results [49], we will also compute the scattering rate $k\sigma(k)$.

III. EFFECTIVE POTENTIALS OF THE $D^{(*)}\bar{B}^{(*)}$ SYSTEMS

A. $D\bar{B}$ systems

As shown in Fig. 1, at LO, there is only a tree-level contact diagram for the scattering process $D(p_1)\bar{B}(p_2) \rightarrow D(p_3)\bar{B}(p_4)$. Using the Lagrangians in Eq. (1), the amplitudes can be written as follows:

$$\mathcal{M}_{(a1)}^{(0)} = 4(D_a + E_a), \quad (17)$$

for isospin $I = 1$, and for isospin $I = 0$

$$\mathcal{M}_{(a1)}^{(0)} = 4(D_a - 3E_a). \quad (18)$$

Next, we consider NLO contributions illustrated in Fig. 1. There are two types of NLO diagrams. The diagrams in Fig. 1 represent one-loop corrections to the LO contact interaction, and the corresponding amplitudes are given by:

$$\mathcal{M}_{a1.1}^{(2)} = -4A(d-1)\frac{g_2^2}{f^2}J_{22}^g, \quad (19)$$

$$\mathcal{M}_{a1.2}^{(2)} = -4A(d-1)\frac{g_1^2}{f^2}J_{22}^g, \quad (20)$$

$$\mathcal{M}_{a1.3}^{(2)} = 4A(d-1)\frac{g_1g_2}{f^2}J_{22}^h, \quad (21)$$

$$\mathcal{M}_{a1.4}^{(2)} = 4A(d-1)\frac{g_1g_2}{f^2}J_{22}^h, \quad (22)$$

$$\mathcal{M}_{a1.5}^{(2)} = -\frac{3}{2}A(d-1)\frac{g_1^2}{f^2}\partial_\omega J_{22}^b, \quad (23)$$

$$\mathcal{M}_{a1.6}^{(2)} = -\frac{3}{2}A(d-1)\frac{g_1^2}{f^2}\partial_\omega J_{22}^b. \quad (24)$$

Here, d represents the space-time dimension, and the coefficient A depends on each diagram and isospin I , which is listed in Table I. The coupling constants g_1 and g_2 refer to the bare coupling constants for the $DD^*\pi$ and $\bar{B}\bar{B}^*\pi$ vertices, respectively.

Using the Lagrangians Eq. (3), the amplitudes for the TPE diagrams in Fig. 1 can be written as

$$\begin{aligned} \mathcal{M}_{c1.1}^{(2)} = & -4\frac{1}{f^4}[A_1(q_0^2J_0^F + J_{22}^F) - A_{15}(q_0^2J_{11}^F + q_0^2J_{21}^F + J_{22}^F) - A_{51}(q_0^2J_{11}^F + q_0^2J_{21}^F + J_{22}^F) + A_5(q_0^2J_0^F + 2q_0^2J_{11}^F \\ & + q_0^2J_{21}^F + J_{22}^F)], \end{aligned} \quad (25)$$

$$\begin{aligned} \mathcal{M}_{c1.2}^{(2)} = & -4i\frac{g_2^2}{f^4}\{A_1[q_0\bar{q}^2J_{22}^T + \bar{q}^2J_{24}^T - (d-1)q_0J_{31}^T + q_0\bar{q}^2J_{32}^T + \bar{q}^2J_{33}^T - (d-1)J_{34}^T] - A_5[q_0\bar{q}^2J_{11}^T - (d-1)q_0J_{21}^T \\ & + 2q_0\bar{q}^2J_{22}^T + \bar{q}^2J_{24}^T - (d-1)q_0J_{31}^T + q_0\bar{q}^2J_{32}^T + \bar{q}^2J_{33}^T - (d-1)J_{34}^T]\}, \end{aligned} \quad (26)$$

$$\begin{aligned} \mathcal{M}_{c1.3}^{(2)} = & -4i\frac{g_2^2}{f^4}\{A_1[q_0\bar{q}^2J_{22}^T + \bar{q}^2J_{24}^T - (d-1)q_0J_{31}^T + q_0\bar{q}^2J_{32}^T + \bar{q}^2J_{33}^T - (d-1)J_{34}^T] - A_5[q_0\bar{q}^2J_{11}^T - (d-1)q_0J_{21}^T \\ & + 2q_0\bar{q}^2J_{22}^T + \bar{q}^2J_{24}^T - (d-1)q_0J_{31}^T + q_0\bar{q}^2J_{32}^T + \bar{q}^2J_{33}^T - (d-1)J_{34}^T]\}, \end{aligned} \quad (27)$$

$$\mathcal{M}_{c1.4}^{(2)} = -4\frac{g_1^2g_2^2}{f^4}A[-\bar{q}^2J_{21}^B + \bar{q}^4J_{22}^B - 2(d+1)\bar{q}^2J_{31}^B + 2\bar{q}^4J_{32}^B + (d^2-1)J_{41}^B - 2(d+1)\bar{q}^2J_{42}^B + \bar{q}^4J_{43}^B], \quad (28)$$

$$\mathcal{M}_{c1.5}^{(2)} = -4\frac{g_1^2g_2^2}{f^4}A[-\bar{q}^2J_{21}^R + \bar{q}^4J_{22}^R - 2(d+1)\bar{q}^2J_{31}^R + 2\bar{q}^4J_{32}^R + (d^2-1)J_{41}^R - 2(d+1)\bar{q}^2J_{42}^R + \bar{q}^4J_{43}^R], \quad (29)$$

where coefficients A_1 , A_{15} , A_{51} and A_5 for each amplitude can be found in Table II.

In the above amplitudes (19)-(29), the loop functions $J_{ij}^{a/b}(m, \omega)$, $J_{ij}^{g/h}(m, \omega_1, \omega_2)$, $J_{ij}^F(m_1, m_2, q)$, $J_{ij}^{T/S}(m_1, m_2, \omega, q)$, and $J_{ij}^{B/R}(m_1, m_2, \omega_1, \omega_2, q)$ are abbreviated as $J_{ij}^{a/b}$, $J_{ij}^{g/h}$, J_{ij}^F , $J_{ij}^{T/S}$, and $J_{ij}^{B/R}$, respectively. The variables m, m_1, m_2 denote the pion mass, while the mass-splitting-dependent variables ω_1 and ω_2 for every amplitudes are collected in Tables I-II. Here we define $\delta_1 = M_{D^*} - M_D$ and $\delta_2 = M_{\bar{B}^*} - M_{\bar{B}}$ as the D^*-D and $\bar{B}^*-\bar{B}$ mass differences, respectively. The calculating procedures of these loop functions follow the Refs. [55, 58].

TABLE I: The coefficients appearing in the contact amplitudes (Eqs.(19)-(24)).

	$I = 1$	$I = 0$	
	A	A	$\omega_1 \quad \omega_2$
$A_{a1.1}$	0	0	$-\delta_2 \quad -\delta_2$
$A_{a1.2}$	0	0	$-\delta_1 \quad -\delta_1$
$A_{a1.3}$	$\frac{1}{4}(D_b + E_b)$	$\frac{1}{4}(-3D_b + 9E_b)$	$-\delta_1 \quad -\delta_2$
$A_{a1.4}$	$\frac{1}{4}(D_b + E_b)$	$\frac{1}{4}(-3D_b + 9E_b)$	$-\delta_1 \quad -\delta_2$
$A_{a1.5}$	$D_a + E_a$	$D_a - 3E_a$	$-\delta_1 \quad 0$
$A_{a1.6}$	$D_a + E_a$	$D_a - 3E_a$	$-\delta_2 \quad 0$

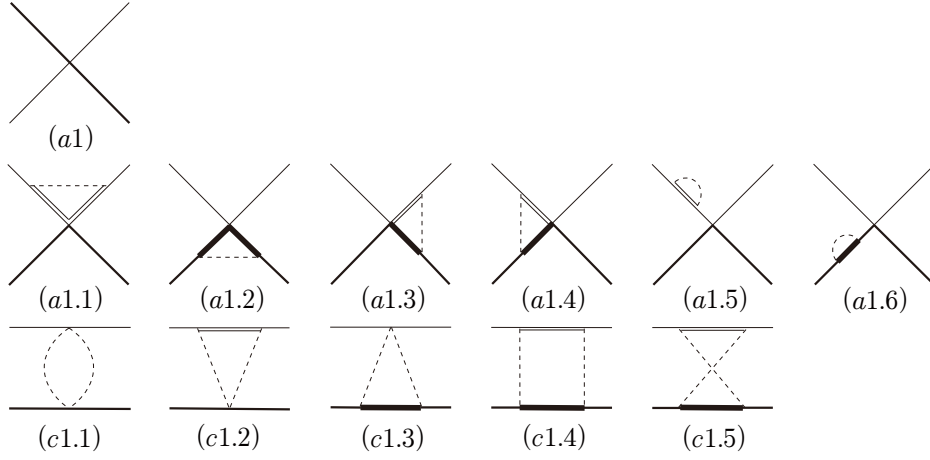


FIG. 1: LO contact, NLO contact and NLO TPE diagrams of the process $D\bar{B} \rightarrow D\bar{B}$. The thin solid, double thin solid, solid, thick solid, and dashed lines stand for the B , B^* , D , D^* and a pion, respectively. TPE diagrams at NLO.

TABLE II: The coefficients appearing in the TPE amplitudes (Eqs. (25)-(29)). Note that we have $A_{51} = A_{15}$.

	$I = 1$			$I = 0$			ω_1	ω_2
	A_1	A_5	A_{15}	A_1	A_5	A_{15}		
$A_{c1.1}$	$\frac{1}{16}$	$\frac{1}{16}$	$-\frac{1}{16}$	$-\frac{3}{16}$	$-\frac{3}{16}$	$\frac{3}{16}$	0	0
$A_{c1.2}$	$\frac{i}{8}$	$-\frac{i}{8}$	0	$-\frac{3i}{8}$	$\frac{3i}{8}$	0	$-\delta_2$	0
$A_{c1.3}$	$\frac{i}{8}$	$-\frac{i}{8}$	0	$-\frac{3i}{8}$	$\frac{3i}{8}$	0	$-\delta_1$	0
$A_{c1.4}$	$\frac{1}{16}$	0	0	$\frac{9}{16}$	0	0	$-\delta_1$	$-\delta_2$
$A_{c1.5}$	$\frac{5}{16}$	0	0	$-\frac{3}{16}$	0	0	$-\delta_1$	$-\delta_2$

B. $D\bar{B}^*$ systems

We now focus on the $D\bar{B}^*$ system. As in the $D\bar{B}$ system, a contact term contributes to the $D\bar{B}^*$ scattering amplitudes at LO, as shown in Fig. 2. For the process $D(p_1)\bar{B}^*(p_2) \rightarrow D(p_3)\bar{B}^*(p_4)$, the scattering amplitude is given by

$$\mathcal{M}_{a2}^{(0)} = -4(D_a + E_a)(\epsilon_2 \cdot \epsilon_4^*), \quad (30)$$

with isospin $I = 1$, and

$$\mathcal{M}_{a2}^{(0)} = -4(D_a - 3E_a)(\epsilon_2 \cdot \epsilon_4^*), \quad (31)$$

with isospin $I = 0$, where ϵ_2 and ϵ_4^* are the polarization vectors of the initial \bar{B}^* and final \bar{B}^* , respectively.

Next, in Fig. 2, we present the one-loop corrections to the contact diagram and the TPE diagrams of the $D\bar{B}^*$ system at NLO. We can calculate the amplitudes for these diagrams using the Feynman rules derived from

the Lagrangian 3. The one-loop correction terms are:

$$\mathcal{M}_{a2.1}^{(2)} = -4\frac{g_2^2}{f^2}AJ_{22}^g(\epsilon_2 \cdot \epsilon_4^*), \quad (32)$$

$$\mathcal{M}_{a2.2}^{(2)} = 4(d-3)(d-2)\frac{g_2^2}{f^2}AJ_{22}^g(\epsilon_2 \cdot \epsilon_4^*), \quad (33)$$

$$\mathcal{M}_{a2.3}^{(2)} = 4(d-1)\frac{g_1^2}{f^2}AJ_{22}^g(\epsilon_2 \cdot \epsilon_4^*), \quad (34)$$

$$\mathcal{M}_{a2.4}^{(2)} = -4\frac{g_1g_2}{f^2}AJ_{22}^h(\epsilon_2 \cdot \epsilon_4^*), \quad (35)$$

$$\mathcal{M}_{a2.5}^{(2)} = -4\frac{g_1g_2}{f^2}AJ_{22}^h(\epsilon_2 \cdot \epsilon_4^*), \quad (36)$$

$$\mathcal{M}_{a2.6}^{(2)} = -4(d-3)(d-2)\frac{g_1g_2}{f^2}AJ_{22}^h(\epsilon_2 \cdot \epsilon_4^*), \quad (37)$$

$$\mathcal{M}_{a2.7}^{(2)} = -4(d-3)(d-2)\frac{g_1g_2}{f^2}AJ_{22}^h(\epsilon_2 \cdot \epsilon_4^*), \quad (38)$$

$$\begin{aligned} \mathcal{M}_{a2.(8+9)}^{(2)} &= \frac{3g_2^2}{2f^2}A[(d-2)\partial_\omega J_{22}^b(\omega_1) + \partial_\omega J_{22}^b(\omega_2)] \\ &\quad \times (\epsilon_2 \cdot \epsilon_4^*), \end{aligned} \quad (39)$$

$$\mathcal{M}_{a2.10}^{(2)} = \frac{3}{2}(d-2)\frac{g_1^2}{2f^2}A\partial_\omega J_{22}^b(\epsilon_2 \cdot \epsilon_4^*). \quad (40)$$

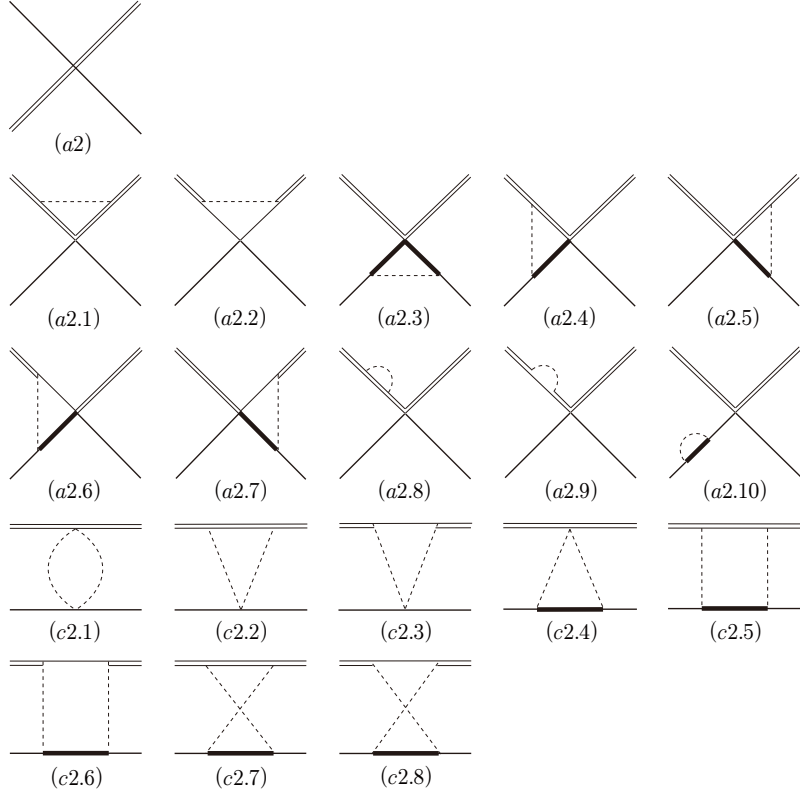


FIG. 2: LO contact, NLO contact and NLO TPE diagrams of the process $D\bar{B}^* \rightarrow D\bar{B}^*$. The thin solid, double thin solid, solid, thick solid, and dashed lines stand for the \bar{B} , B^* , D , D^* and a pion, respectively.

The TPE diagrams consist of football, triangle, planar, and crossed box diagrams. The corresponding amplitudes are given by:

$$\mathcal{M}_{c2.1}^{(2)} = 4 \frac{1}{f^4} [A_1(q_0^2 J_0^F + J_{22}^F) + A_{15}(q_0^2 J_{11}^F + q_0^2 J_{21}^F + J_{22}^F) - A_{51}(q_0^2 J_{11}^F + q_0^2 J_{21}^F + J_{22}^F) + A_5(q_0^2 J_0^F + 2q_0^2 J_{11}^F + q_0^2 J_{21}^F + J_{22}^F)] \epsilon_2 \cdot \epsilon_4^*, \quad (41)$$

$$\mathcal{M}_{c2.2}^{(2)} = i4 \frac{g_2^2}{f^4} \{ [A_1(q_0 J_{22}^S + J_{24}^S + q_0 J_{32}^S + J_{33}^S) - A_5(q_0 J_{11}^S + 2q_0 J_{22}^S + J_{24}^S + q_0 J_{32}^S + J_{33}^S)] (q \cdot \epsilon_2)(q \cdot \epsilon_4^*) + [A_1(q_0 J_{31}^S + J_{34}^S) - A_5(q_0 J_{21}^S + q_0 J_{31}^S + J_{34}^S)] (\epsilon_2 \cdot \epsilon_4^*) \}, \quad (42)$$

$$\mathcal{M}_{c2.3}^{(2)} = -i4 \frac{g_2^2}{f^4} (d-3) [A_1(q_0 J_{22}^S + J_{24}^S + q_0 J_{32}^S + J_{33}^S) - A_5(q_0 J_{11}^S + 2q_0 J_{22}^S + J_{24}^S + q_0 J_{32}^S + J_{33}^S)] (q \cdot \epsilon_2)(q \cdot \epsilon_4^*) - i4 \frac{g_2^2}{f^4} (d-3) \{ A_1[q_0 \bar{q}^2 J_{22}^S + \bar{q}^2 J_{24}^S + (2-d)q_0 J_{31}^S + q_0 \bar{q}^2 J_{32}^S + \bar{q}^2 J_{33}^S + (2-d)J_{34}^S] - A_5[q_0 \bar{q}^2 J_{11}^S + (2-d)q_0(J_{21}^S + J_{31}^S) + 2q_0 \bar{q}^2 J_{22}^S + \bar{q}^2 J_{24}^S + q_0 \bar{q}^2 J_{32}^S + \bar{q}^2 J_{33}^S + (2-d)J_{34}^S] \} (\epsilon_2 \cdot \epsilon_4^*), \quad (43)$$

$$\mathcal{M}_{c2.4}^{(2)} = -i4 \frac{g_1^2}{f^4} \{ A_1[q_0 \bar{q}^2 J_{22}^T + \bar{q}^2 J_{24}^T + (1-d)q_0 J_{31}^T + q_0 \bar{q}^2 J_{32}^T + \bar{q}^2 J_{33}^T + (1-d)J_{34}^T] - A_5[q_0 \bar{q}^2 J_{11}^T + (1-d)q_0(J_{21}^T + J_{31}^T) + 2q_0 \bar{q}^2 J_{22}^T + \bar{q}^2 J_{24}^T + q_0 \bar{q}^2 J_{32}^T + \bar{q}^2 J_{33}^T + (1-d)J_{34}^T] \} (\epsilon_2 \cdot \epsilon_4^*), \quad (44)$$

$$\mathcal{M}_{c2.5}^{(2)} = -iA_{14} i \frac{g_1^2 g_2^2}{f^4} \{ [J_{21}^B - \bar{q}^2 J_{22}^B + (d+3)(J_{31}^B + J_{42}^B) - 2\bar{q}^2 J_{32}^B - \bar{q}^2 J_{43}^B] (q \cdot \epsilon_2)(q \cdot \epsilon_4^*) - [\bar{q}^2 (J_{31}^B + J_{42}^B) - (1+d)J_{41}^B] \} (\epsilon_2 \cdot \epsilon_4^*), \quad (45)$$

$$\begin{aligned} \mathcal{M}_{c2.6}^{(2)} = & -iA_1 4i \frac{g_1^2 g_2^2}{f^4} (d-3) \{ [J_{21}^B - \bar{q}^2 J_{22}^B + (d+3)J_{31}^B - 2\bar{q}^2 J_{32}^B + (d+3)J_{42}^B - \bar{q}^2 J_{43}^B] (q \cdot \epsilon_2) (q \cdot \epsilon_4^*) \\ & + [-\bar{q}^2 J_{21}^B + \bar{q}^4 J_{22}^B - (2d+1)\bar{q}^2 (J_{31}^B + J_{42}^B) + 2\bar{q}^4 J_{32}^B + (d+1)(d-2)J_{41}^B + \bar{q}^4 J_{43}^B] \} (\epsilon_2 \cdot \epsilon_4^*), \end{aligned} \quad (46)$$

$$\begin{aligned} \mathcal{M}_{c2.7}^{(2)} = & -iA_1 4i \frac{g_1^2 g_2^2}{f^4} \{ [J_{21}^R - \bar{q}^2 J_{22}^R + (d+3)(J_{31}^R + J_{42}^R) - 2\bar{q}^2 J_{32}^R - \bar{q}^2 J_{43}^R] (q \cdot \epsilon_2) (q \cdot \epsilon_4^*) - [\bar{q}^2 J_{31}^R \\ & - (1+d)J_{41}^R + \bar{q}^2 J_{42}^R] \} (\epsilon_2 \cdot \epsilon_4^*), \end{aligned} \quad (47)$$

$$\begin{aligned} \mathcal{M}_{c2.8}^{(2)} = & -i4i \frac{g_1^2 g_2^2}{f^4} (d-3) A_1 \{ [J_{21}^R - \bar{q}^2 J_{22}^R + (d+3)J_{31}^R - 2\bar{q}^2 J_{32}^R + 3J_{42}^R - \bar{q}^2 J_{43}^R] (q \cdot \epsilon_2) (q \cdot \epsilon_4^*) + [-\bar{q}^2 J_{21}^R \\ & + \bar{q}^4 J_{22}^R - (2d+1)\bar{q}^2 (J_{31}^R + J_{42}^R) + 2\bar{q}^4 J_{32}^R + (d+1)(d-2)J_{41}^R + \bar{q}^4 J_{43}^R] \} (\epsilon_2 \cdot \epsilon_4^*), \end{aligned} \quad (48)$$

The coefficients in the above expressions are listed in Tables III and IV. In this work, we focus on the S -wave interactions, so we replace the terms $\epsilon_2 \cdot \epsilon_4^*$ and $(q \cdot \epsilon_2)(q \cdot \epsilon_4^*)$ in the equations with [55, 57, 58]

$$(\epsilon_2 \cdot \epsilon_4^*) \mapsto -1, \quad (q \cdot \epsilon_2)(q \cdot \epsilon_4^*) \mapsto \frac{1}{d-1} \bar{q}^2. \quad (49)$$

TABLE III: The coefficients in the NLO contact amplitudes in Eqs.(32)-(40)

	$I = 1$	$I = 0$	ω_1	ω_2
	A	A		
$A_{a2.1}$	$\frac{1}{4}(3D_a - E_a)$	$\frac{3}{4}(D_a + E_a)$	δ_2	δ_2
$A_{a2.2}$	$\frac{1}{4}(3D_a - E_a)$	$\frac{3}{4}(D_a + E_a)$	0	0
$A_{a2.3}$	0	0	$-\delta_1$	$-\delta_1$
$A_{a2.4}$	$\frac{1}{4}(D_b + E_b)$	$\frac{-3}{4}(D_b - 3E_b)$	δ_2	$-\delta_1$
$A_{a2.5}$	$\frac{1}{4}(D_b + E_b)$	$\frac{-3}{4}(D_b - 3E_b)$	$-\delta_1$	δ_2
$A_{a2.6}$	$\frac{1}{4}(D_b + E_b)$	$\frac{-3}{4}(D_b - 3E_b)$	δ_2	$-\delta_1$
$A_{a2.7}$	$\frac{1}{4}(D_b + E_b)$	$\frac{-3}{4}(D_b - 3E_b)$	$-\delta_1$	δ_2
$A_{a2.(8+9)}$	$D_a + E_a$	$D_a - 3E_a$	0	δ_2
$A_{a2.10}$	$D_a + E_a$	$D_a - 3E_a$	δ_1	0

C. $D^* \bar{B}^*$ systems

Next, we consider the $D^* \bar{B}^*$ systems. At LO, both the contact and OPE diagrams contribute to the scattering amplitudes, as shown in Fig. 3. At NLO, there are one-loop corrections to the LO diagrams and newly appeared TPE diagrams shown in Fig. 3. Compared to the

$D\bar{B}$ and $D\bar{B}^*$ systems, the $D^* \bar{B}^*$ systems include significantly more diagrams, resulting in more complex interactions. The corresponding scattering amplitudes for these diagrams are listed in Eqs. (50)-(53) and Eqs. (57)-(98).

At LO, utilizing the Lagrangian presented in Eq. (1) and Eq. (3), the contact and OPE contributions of the scattering process $D^*(p_1) \bar{B}^*(p_2) \rightarrow D^*(p_3) \bar{B}^*(p_4)$ depicted in Fig. 3 read

$$\begin{aligned} \mathcal{M}_{a3}^{(0)} = & 8[(D_a - D_b + E_a - E_b)(\mathcal{O}_1 + \mathcal{O}_2) \\ & + 2(D_b + E_b)\mathcal{O}_3], \end{aligned} \quad (50)$$

$$\mathcal{M}_{b3}^{(0)} = -\frac{g^2}{f^2} \frac{\mathcal{G}(q, \epsilon_1, \epsilon_2, \epsilon_3^*, \epsilon_4^*)}{q^2 - m_\pi^2}, \quad (51)$$

for isospin $I = 1$. And we have

$$\begin{aligned} \mathcal{M}_{(a3)}^{(0)} = & 8[(D_a - D_b + E_a - E_b)(\mathcal{O}_1 + \mathcal{O}_2) \\ & + 2(D_b + E_b)\mathcal{O}_3], \end{aligned} \quad (52)$$

$$\mathcal{M}_{(b3)}^{(0)} = -\frac{g^2}{f^2} \frac{\mathcal{G}(q, \epsilon_1, \epsilon_2, \epsilon_3^*, \epsilon_4^*)}{q^2 - m_\pi^2}, \quad (53)$$

for isospin $I = 0$.

Here, $\epsilon_1(\epsilon_2)$ and $\epsilon_3^*(\epsilon_4^*)$ stand for the polarization vectors of the initial $D^*(\bar{B}^*)$ and final $D^*(\bar{B}^*)$ mesons, respectively. For convenience, we define

$$\begin{aligned} \mathcal{O}_1 = & (\epsilon_1 \cdot \epsilon_3^*)(\epsilon_2 \cdot \epsilon_4^*), \quad \mathcal{O}_2 = (\epsilon_1 \cdot \epsilon_4^*)(\epsilon_2 \cdot \epsilon_3^*), \\ \mathcal{O}_3 = & (\epsilon_1 \cdot \epsilon_2)(\epsilon_3^* \cdot \epsilon_4^*), \quad \mathcal{O}_2^a = (q \cdot \epsilon_3^*)(q \cdot \epsilon_2)(\epsilon_1 \cdot \epsilon_4^*), \\ \mathcal{O}_2^b = & (q \cdot \epsilon_1)(q \cdot \epsilon_4^*)(\epsilon_2 \cdot \epsilon_3^*), \\ \mathcal{O}_3^a = & (q \cdot \epsilon_3^*)(q \cdot \epsilon_4^*)(\epsilon_1 \cdot \epsilon_2), \\ \mathcal{O}_3^b = & (q \cdot \epsilon_1)(q \cdot \epsilon_2)(\epsilon_3^* \cdot \epsilon_4^*), \end{aligned} \quad (54)$$

and

$$\begin{aligned} \mathcal{G}(q, \epsilon_1, \epsilon_2, \epsilon_3^*, \epsilon_4^*) = & \bar{q}^2(\mathcal{O}_2 - \mathcal{O}_3) + (\mathcal{O}_2^a - \mathcal{O}_3^a) \\ & + (\mathcal{O}_2^b - \mathcal{O}_3^b). \end{aligned} \quad (55)$$

TABLE IV: The coefficients in the TPE amplitudes (Eqs. (41)-(48)). Note that we have $A_{51} = A_{15}$.

	$I = 1$			$I = 0$			ω_1	ω_2
	A_1	A_5	A_{15}	A_1	A_5	A_{15}		
$A_{c2.1}$	$\frac{1}{16}$	$\frac{1}{16}$	$-\frac{1}{16}$	$-\frac{3}{16}$	$-\frac{3}{16}$	$\frac{3}{16}$	0	0
$A_{c2.2}$	$\frac{i}{8}$	$\frac{i}{8}$	0	$-\frac{3i}{8}$	$\frac{3i}{8}$	0	δ_2	0
$A_{c2.2}$	$\frac{i}{8}$	$\frac{i}{8}$	0	$-\frac{3i}{8}$	$\frac{3i}{8}$	0	δ_2	0
$A_{c2.3}$	$\frac{i}{8}$	$-\frac{i}{8}$	0	$-\frac{3i}{8}$	$\frac{3i}{8}$	0	0	0
$A_{c2.4}$	$\frac{i}{8}$	$-\frac{i}{8}$	0	$-\frac{3i}{8}$	$\frac{3i}{8}$	0	$-\delta_1$	0
$A_{c2.5}$	$\frac{1}{16}$	0	0	$\frac{9}{16}$	0	0	$-\delta_1$	δ_2
$A_{c2.6}$	$\frac{1}{16}$	0	0	$\frac{9}{16}$	0	0	$-\delta_1$	0
$A_{c2.7}$	$\frac{5}{16}$	0	0	$-\frac{3}{16}$	0	0	$-\delta_1$	δ_2
$A_{c2.8}$	$\frac{5}{16}$	0	0	$-\frac{3}{16}$	0	0	$-\delta_1$	0

Similar to the definitions (54), we also define

$$\begin{aligned}
\mathcal{O}_1^a &= (q \cdot \epsilon_1)(q \cdot \epsilon_3^*)(\epsilon_2 \cdot \epsilon_4^*), \\
\mathcal{O}_1^b &= (q \cdot \epsilon_2)(q \cdot \epsilon_4^*)(\epsilon_1 \cdot \epsilon_3^*), \\
\mathcal{O}_1^c &= (q \cdot \epsilon_1)(q \cdot \epsilon_3^*)(q \cdot \epsilon_2)(q \cdot \epsilon_4^*), \\
\mathcal{O}_3^c &= (q \cdot \epsilon_1)(q \cdot \epsilon_2)(q \cdot \epsilon_3^*)(q \cdot \epsilon_4^*).
\end{aligned} \tag{56}$$

The one-loop corrections to the contact amplitudes are listed as follows:

$$\begin{aligned}
\mathcal{M}_{a3.1}^{(2)} &= -4 \frac{g_2^2}{f^2} [(d-3)(d-2)A_1\mathcal{O}_1 - (d-3)A_2\mathcal{O}_2 \\
&\quad + (d-3)A_3\mathcal{O}_3] J_{22}^g,
\end{aligned} \tag{57}$$

$$\mathcal{M}_{a3.2}^{(2)} = -4 \frac{g_2^2}{f^2} A_1\mathcal{O}_1 J_{22}^g, \tag{58}$$

$$\mathcal{M}_{a3.3}^{(2)} = -4 \frac{g_2^2}{f^2} (d-3)[A_1\mathcal{O}_2 - A_2\mathcal{O}_3] J_{22}^g, \tag{59}$$

$$\mathcal{M}_{a3.4}^{(2)} = -4 \frac{g_2^2}{f^2} (d-3)[A_1\mathcal{O}_2 - A_2\mathcal{O}_3] J_{22}^g, \tag{60}$$

$$\begin{aligned}
\mathcal{M}_{a3.5}^{(2)} &= -4 \frac{g_1^2}{f^2} [(d-3)(d-2)A_1\mathcal{O}_1 - (d-3)A_2\mathcal{O}_2 \\
&\quad + (d-3)A_3\mathcal{O}_3] J_{22}^g,
\end{aligned} \tag{61}$$

$$\mathcal{M}_{a3.6}^{(2)} = -4 \frac{g_1^2}{f^2} A_1\mathcal{O}_1 J_{22}^g, \tag{62}$$

$$\mathcal{M}_{a3.7}^{(2)} = -4 \frac{g_1^2}{f^2} (d-3)[A_1\mathcal{O}_2 - A_2\mathcal{O}_3] J_{22}^g, \tag{63}$$

$$\mathcal{M}_{a3.8}^{(2)} = -4 \frac{g_1^2}{f^2} (d-3)[A_1\mathcal{O}_2 - A_2\mathcal{O}_3] J_{22}^g, \tag{64}$$

$$\mathcal{M}_{a3.9}^{(2)} = 4 \frac{g_1 g_2}{f^2} (d-3)[A_1\mathcal{O}_1 - A_2\mathcal{O}_2 + A_3\mathcal{O}_3] J_{22}^h, \tag{65}$$

$$\mathcal{M}_{a3.10}^{(2)} = 4 \frac{g_1^2}{f^2} A_1\mathcal{O}_3 J_{22}^h, \tag{66}$$

$$\mathcal{M}_{a3.11}^{(2)} = 4 \frac{g_1^2}{f^2} (d-3)[A_1\mathcal{O}_1 - A_2\mathcal{O}_2] J_{22}^h, \tag{67}$$

$$\mathcal{M}_{a3.12}^{(2)} = 4 \frac{g_1^2}{f^2} (d-3)[A_1\mathcal{O}_1 - A_2\mathcal{O}_2] J_{22}^h, \tag{68}$$

$$\mathcal{M}_{a3.13}^{(2)} = 4 \frac{g_1 g_2}{f^2} (d-3)[A_1\mathcal{O}_1 - A_2\mathcal{O}_2 + A_3\mathcal{O}_3] J_{22}^h, \tag{69}$$

$$\mathcal{M}_{a3.14}^{(2)} = 4 \frac{g_1 g_2}{f^2} A_1\mathcal{O}_3 J_{22}^h, \tag{70}$$

$$\mathcal{M}_{a3.15}^{(2)} = 4 \frac{g_1 g_2}{f^2} (d-3)[A_1\mathcal{O}_1 - A_2\mathcal{O}_2] J_{22}^h, \tag{71}$$

$$\mathcal{M}_{a3.16}^{(2)} = 4 \frac{g_1 g_2}{f^2} (d-3)[A_1\mathcal{O}_1 - A_2\mathcal{O}_2] J_{22}^h, \tag{72}$$

$$\mathcal{M}_{a3.(17+18)}^{(2)} = -\frac{3}{8} \frac{g_2^2}{f^2} A_1 [(d-2)\partial_\omega J_{22}^b(\omega_1) + \partial_\omega J_{22}^b(\omega_2)], \tag{73}$$

$$\mathcal{M}_{a3.(19+20)}^{(2)} = -\frac{3}{8} \frac{g_1^2}{f^2} A_1 [(d-2)\partial_\omega J_{22}^b(\omega_1) + \partial_\omega J_{22}^b(\omega_2)], \tag{74}$$

where coefficients appearing in the above contact amplitudes are shown in Table VI.

Next, we consider the NLO one-pion-exchange interactions in the D^*B^* systems. The corresponding diagrams

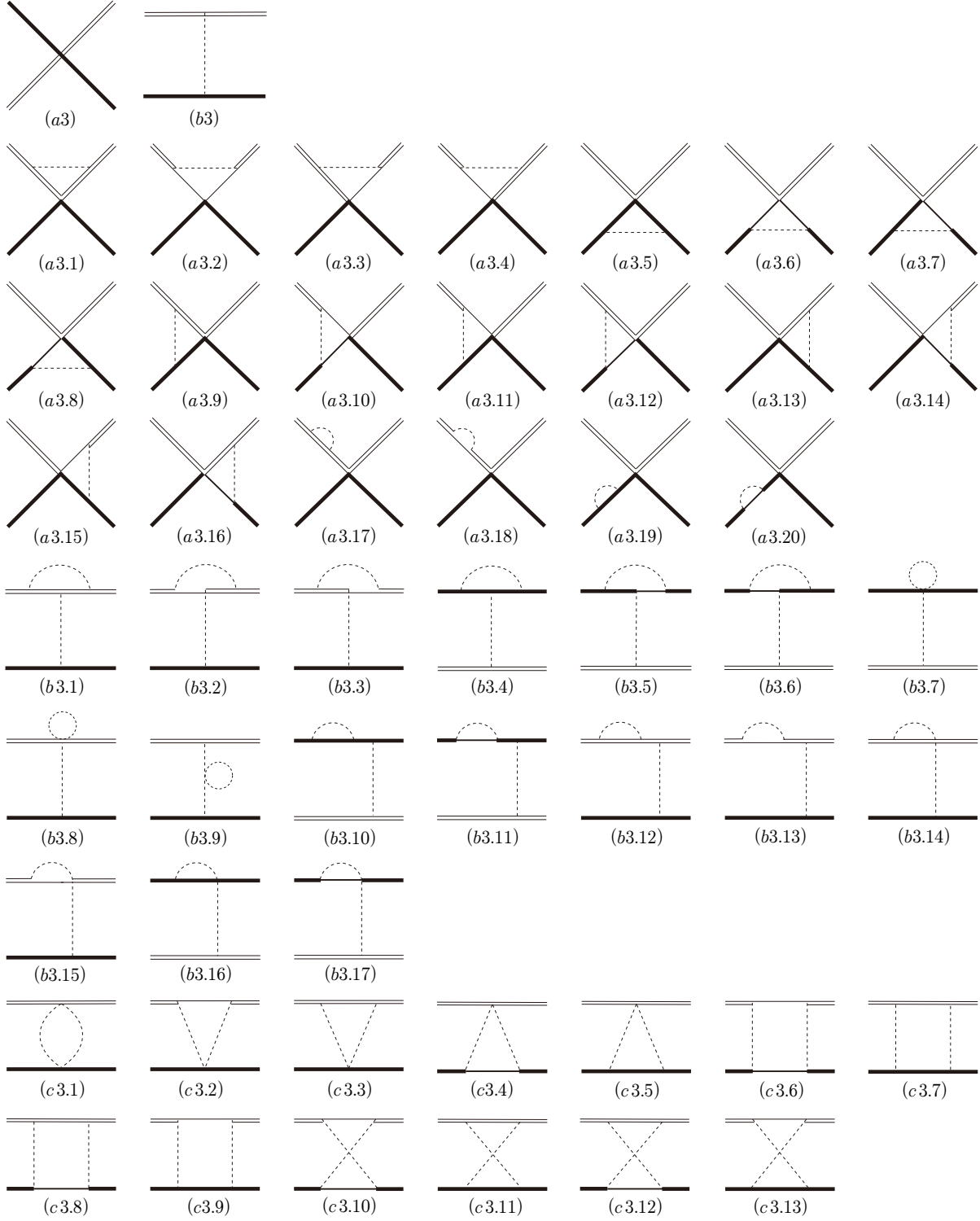


FIG. 3: LO contact, LO OPE, NLO contact, NLO OPE, and NLO TPE diagrams of the process $D^* \bar{B}^* \rightarrow D^* \bar{B}^*$. The thin solid, double thin solid, solid, thick solid, and dashed lines stand for the \bar{B} , \bar{B}^* , D , D^* , and a pion, respectively.

are illustrated in Fig. 3, and the amplitudes:

$$\mathcal{M}_{b3.1}^{(2)} = 4 \frac{g_1^3 g_2}{f^2} A_1 J_{22}^g \frac{\mathcal{G}(q, \epsilon_1, \epsilon_2, \epsilon_3^*, \epsilon_4^*)}{q^2 - m_\pi^2}, \quad (75)$$

$$\mathcal{M}_{b3.2}^{(2)} = -4 \frac{g_1^3 g_2}{f^2} A_1 J_{22}^g \frac{\mathcal{G}(q, \epsilon_1, \epsilon_2, \epsilon_3^*, \epsilon_4^*)}{q^2 - m_\pi^2}, \quad (76)$$

$$\mathcal{M}_{b3.3}^{(2)} = -4 \frac{g_1^3 g_2}{f^2} A_1 J_{22}^g \frac{\mathcal{G}(q, \epsilon_1, \epsilon_2, \epsilon_3^*, \epsilon_4^*)}{q^2 - m_\pi^2}, \quad (77)$$

$$\mathcal{M}_{b3.4}^{(2)} = 4 \frac{g_1 g_2^3}{f^2} A_1 J_{22}^g \frac{\mathcal{G}(q, \epsilon_1, \epsilon_2, \epsilon_3^*, \epsilon_4^*)}{q^2 - m_\pi^2}, \quad (78)$$

$$\mathcal{M}_{b3.5}^{(2)} = 4 \frac{g_1 g_2^3}{f^2} A_1 J_{22}^g \frac{\mathcal{G}(q, \epsilon_1, \epsilon_2, \epsilon_3^*, \epsilon_4^*)}{q^2 - m_\pi^2}, \quad (79)$$

$$\mathcal{M}_{b3.6}^{(2)} = 4 \frac{g_1 g_2^3}{f^2} A_1 J_{22}^g \frac{\mathcal{G}(q, \epsilon_1, \epsilon_2, \epsilon_3^*, \epsilon_4^*)}{q^2 - m_\pi^2}, \quad (80)$$

$$\mathcal{M}_{b3.7}^{(2)} = -\frac{8}{3} \frac{g_1 g_2}{f^2} A_1 J_0^c \frac{\mathcal{G}(q, \epsilon_1, \epsilon_2, \epsilon_3^*, \epsilon_4^*)}{q^2 - m_\pi^2}, \quad (81)$$

$$\mathcal{M}_{b3.8}^{(2)} = -\frac{8}{3} \frac{g_1 g_2}{f^2} A_1 J_0^c \frac{\mathcal{G}(q, \epsilon_1, \epsilon_2, \epsilon_3^*, \epsilon_4^*)}{q^2 - m_\pi^2}, \quad (82)$$

$$\begin{aligned} \mathcal{M}_{b3.9}^{(2)} &= -\frac{8}{3} \frac{g_1 g_2}{f^2} A_1 [2m^2 L + \frac{m^2}{16\pi^2} \log(\frac{m^2}{\mu^2})] \\ &\times \frac{\mathcal{G}(q, \epsilon_1, \epsilon_2, \epsilon_3^*, \epsilon_4^*)}{q^2 - m_\pi^2}, \end{aligned} \quad (83)$$

$$\begin{aligned} \mathcal{M}_{b3.(10+11)}^{(2)} &= \frac{3g_1 g_2^3}{2f^2} A_1 [(d-2)\partial_\omega J_{22}^b(\omega_1) + \partial_\omega J_{22}^b(\omega_2)] \\ &\times \frac{\mathcal{G}(q, \epsilon_1, \epsilon_2, \epsilon_3^*, \epsilon_4^*)}{q^2 - m_\pi^2}, \end{aligned} \quad (84)$$

$$\begin{aligned} \mathcal{M}_{b3.(12+13)}^{(2)} &= \frac{3g_1 g_2^3}{2f^2} A_1 [(d-2)\partial_\omega J_{22}^b(\omega_1) + \partial_\omega J_{22}^b(\omega_2)] \\ &\times \frac{\mathcal{G}(q, \epsilon_1, \epsilon_2, \epsilon_3^*, \epsilon_4^*)}{q^2 - m_\pi^2}, \end{aligned} \quad (85)$$

$$\mathcal{M}_{b3.14}^{(2)} = \mathcal{M}_{b3.15}^{(2)} = \mathcal{M}_{b3.16}^{(2)} = \mathcal{M}_{b3.17}^{(2)} = 0. \quad (86)$$

The amplitudes for the TPE diagrams shown in Fig. 3 are calculated to be

$$\mathcal{M}_{c3.1}^{(2)} = -4 \frac{1}{f^4} [A_1(q_0^2 J_{21}^F + J_{22}^F) - (A_{15} + A_{51} + A_5)(q_0^2 J_{11}^F + q_0^2 J_{21}^F + J_{22}^F) + A_5(q_0^2 J_0^F + q_0^2 J_{11}^F)] \mathcal{O}_1, \quad (87)$$

$$\begin{aligned} \mathcal{M}_{c3.2}^{(2)} &= -i4 \frac{g_2^2}{f^4} \{ [A_1(q_0 J_{22}^S + J_{24}^S + q_0 J_{32}^S + J_{33}^S) - A_5(q_0 J_{11}^S + 2q_0 J_{22}^S + J_{24}^S + q_0 J_{32}^S + J_{33}^S)] \mathcal{O}_1^a + [A_1(q_0 J_{31}^S + J_{34}^S) \\ &- A_5(q_0 J_{21}^S + q_0 J_{31}^S + J_{34}^S)] \mathcal{O}_1 \}, \end{aligned} \quad (88)$$

$$\begin{aligned} \mathcal{M}_{c3.3}^{(2)} &= i4 \frac{g_2^2}{f^4} (d-3) [A_1(q_0 J_{22}^S + J_{24}^S + q_0 J_{32}^S + J_{33}^S) - A_5(q_0 J_{11}^S + 2q_0 J_{22}^S + J_{24}^S + q_0 J_{32}^S + J_{33}^S)] \mathcal{O}_1^a \\ &+ i4 \frac{g_2^2}{f^4} (d-3) \{ A_1 [(q_0 \bar{q}^2 J_{22}^S + \bar{q}^2 J_{24}^S + (2-d)q_0 J_{31}^S + q_0 \bar{q}^2 J_{32}^S + \bar{q}^2 J_{33}^S + (2-d)q_0 J_{34}^S)] \\ &- A_5 [q_0 \bar{q}^2 J_{11}^S + (2-d)q_0 J_{21}^S + \bar{q}^2 J_{24}^S + (2-d)q_0 J_{31}^S + q_0 \bar{q}^2 J_{32}^S + \bar{q}^2 J_{33}^S + (2-d)q_0 J_{34}^S] \} \mathcal{O}_1, \end{aligned} \quad (89)$$

$$\begin{aligned} \mathcal{M}_{c3.4}^{(2)} &= i4 \frac{g_1^2}{f^4} \{ [A_1(q_0 J_{22}^T + J_{24}^T + q_0 J_{32}^T + J_{33}^T) - A_5(q_0 J_{11}^T + 2q_0 J_{22}^T + J_{24}^T + q_0 J_{32}^T + J_{33}^T)] \mathcal{O}_1^b + [A_1(q_0 J_{31}^T + J_{34}^T) \\ &- A_5(q_0 J_{21}^T + q_0 J_{31}^T + J_{34}^T)] \mathcal{O}_1 \}, \end{aligned} \quad (90)$$

$$\begin{aligned} \mathcal{M}_{c3.5}^{(2)} &= -i4 \frac{g_1^2}{f^4} (d-3) [A_1(q_0 J_{22}^T + J_{24}^T + q_0 J_{32}^T + J_{33}^T) - A_5(q_0 J_{11}^T + 2q_0 J_{22}^T + J_{24}^T + q_0 J_{32}^T + J_{33}^T)] \mathcal{O}_1^a \\ &- i4 \frac{g_1^2}{f^4} (d-3) \{ A_1 [(q_0 \bar{q}^2 J_{22}^T + \bar{q}^2 J_{24}^T + (2-d)q_0 J_{31}^T + q_0 \bar{q}^2 J_{32}^T + \bar{q}^2 J_{33}^T + (2-d)q_0 J_{34}^T)] \\ &- A_5 [q_0 \bar{q}^2 J_{11}^T + (2-d)q_0 J_{21}^T + \bar{q}^2 J_{24}^T + (2-d)q_0 J_{31}^T + q_0 \bar{q}^2 J_{32}^T + \bar{q}^2 J_{33}^T + (2-d)q_0 J_{34}^T] \} \mathcal{O}_1, \end{aligned} \quad (91)$$

$$\begin{aligned} \mathcal{M}_{c3.6}^{(2)} = & -4 \frac{g_1^2 g_2^2}{f^4} A_1 [(\mathcal{O}_1 + \mathcal{O}_2 + \mathcal{O}_3) J_{41}^B + \mathcal{O}_3^b (J_{21}^B + 2J_{31}^B + J_{42}^B) + (\mathcal{O}_1^a + \mathcal{O}_1^b + \mathcal{O}_2^a + \mathcal{O}_2^b) (J_{31}^B + J_{42}^B) + \mathcal{O}_3^a J_{42}^B \\ & + \mathcal{O}_3^c (J_{22}^B + 2J_{32}^B + J_{43}^B)], \end{aligned} \quad (92)$$

$$\begin{aligned} \mathcal{M}_{c3.7}^{(2)} = & -4 \frac{g_1^2 g_2^2}{f^4} (d-3)^2 A_1 \{[(d-2)(d-1)\mathcal{O}_1 + \mathcal{O}_2 + \mathcal{O}_3] J_{41}^B + (\bar{q}^4 \mathcal{O}_1 + \bar{q}^2 \mathcal{O}_1^a + \bar{q}^2 \mathcal{O}_1^b + \mathcal{O}_1^c) (J_{22}^B + 2J_{32}^B + J_{43}^B) \\ & - (\bar{q}^2 \mathcal{O}_1 + \mathcal{O}_1^a + \mathcal{O}_1^b - \mathcal{O}_3^a) J_{21}^B - [2d\bar{q}^2 \mathcal{O}_1 + (d+2)\mathcal{O}_1^a + (d+2)\mathcal{O}_1^b - \mathcal{O}_2^a - \mathcal{O}_2^b - \mathcal{O}_3^b] (J_{31}^B + J_{42}^B) \\ & + \mathcal{O}_3^b J_{31}^B + \mathcal{O}_3^a J_{42}^B\}, \end{aligned} \quad (93)$$

$$\begin{aligned} \mathcal{M}_{c3.8}^{(2)} = & 4 \frac{g_1^2 g_2^2}{f^4} (d-3) A_1 \{(-d\mathcal{O}_1 + \mathcal{O}_2 + \mathcal{O}_3) J_{41}^B + (\bar{q}^2 \mathcal{O}_1^b + \mathcal{O}_3^c) (J_{22}^B + 2J_{32}^B + J_{43}^B) + (\mathcal{O}_2^b - \mathcal{O}_1^b) J_{21}^B \\ & + [\bar{q}^2 \mathcal{O}_1 + \mathcal{O}_1^a - (d+2)\mathcal{O}_1^b + \mathcal{O}_2^b + \mathcal{O}_3^a + \mathcal{O}_3^b] (J_{31}^B + J_{42}^B) + \mathcal{O}_2^b J_{31}^B + \mathcal{O}_2^a J_{42}^B\}, \end{aligned} \quad (94)$$

$$\begin{aligned} \mathcal{M}_{c3.9}^{(2)} = & 4 \frac{g_1^2 g_2^2}{f^4} (d-3) A_1 \{(-d\mathcal{O}_1 + \mathcal{O}_2 + \mathcal{O}_3) J_{41}^B + (\bar{q}^2 \mathcal{O}_1^a + \mathcal{O}_3^c) (J_{22}^B + 2J_{32}^B + J_{43}^B) + (\mathcal{O}_2^a - \mathcal{O}_1^a) J_{21}^B \\ & + [\bar{q}^2 \mathcal{O}_1 - (d+2)\mathcal{O}_1^a + \mathcal{O}_1^b + \mathcal{O}_2^a + \mathcal{O}_3^a + \mathcal{O}_3^b] (J_{31}^B + J_{42}^B) + \mathcal{O}_2^a J_{31}^B + \mathcal{O}_2^b J_{42}^B\}, \end{aligned} \quad (95)$$

$$\mathcal{M}_{c3.10}^{(2)} = 5\mathcal{M}_{c3.6}^{(2)}/\{J^B \rightarrow J^R\}, \quad \mathcal{M}_{c3.11}^{(2)} = 5\mathcal{M}_{c3.7}^{(2)}/\{J^B \rightarrow J^R\}, \quad (96)$$

$$\begin{aligned} \mathcal{M}_{c2.12}^{(2)} = & 4 \frac{g_1^2 g_2^2}{f^4} (d-3) A_1 \{(-d\mathcal{O}_1 + \mathcal{O}_2 + \mathcal{O}_3) J_{41}^R + (\bar{q}^2 \mathcal{O}_1^b + \mathcal{O}_3^c) (J_{22}^R + 2J_{32}^R + J_{43}^R) + (\mathcal{O}_2^b - \mathcal{O}_1^b) J_{21}^R \\ & + [\bar{q}^2 \mathcal{O}_1 + \mathcal{O}_1^a - (d+2)\mathcal{O}_1^b + \mathcal{O}_2^a + \mathcal{O}_3^a + \mathcal{O}_3^b] (J_{31}^R + J_{42}^R) + \mathcal{O}_3^b J_{31}^R + \mathcal{O}_3^a J_{42}^R\}, \end{aligned} \quad (97)$$

$$\begin{aligned} \mathcal{M}_{c3.13}^{(2)} = & 4 \frac{g_1^2 g_2^2}{f^4} (d-3) A_1 \{(-d\mathcal{O}_1 + \mathcal{O}_2 + \mathcal{O}_3) J_{41}^R + (\bar{q}^2 \mathcal{O}_1^a + \mathcal{O}_3^c) (J_{22}^R + 2J_{32}^R + J_{43}^R) + (\mathcal{O}_2^a - \mathcal{O}_1^a) J_{21}^R \\ & + [\bar{q}^2 \mathcal{O}_1 + \mathcal{O}_1^a - (d+2)\mathcal{O}_1^b + \mathcal{O}_2^a + \mathcal{O}_3^a + \mathcal{O}_3^b] (J_{31}^R + J_{42}^R) + \mathcal{O}_3^a J_{31}^R + \mathcal{O}_3^b J_{42}^R\}, \end{aligned} \quad (98)$$

To further evaluate the calculated amplitudes, we should deal with the terms (54) according to the partial wave we considered. In S -wave, for the terms like $(q \cdot \epsilon_i)(q \cdot \epsilon_j^*)(\epsilon_k \cdot \epsilon_l^*)$ we can make the following substitutions:

$$\begin{aligned} (\epsilon_i \cdot \epsilon_j)(q \cdot \epsilon_k)(q \cdot \epsilon_l) & \mapsto -\frac{1}{d-1} \bar{q}^2 (\epsilon_i \cdot \epsilon_j)(\epsilon_k \cdot \epsilon_l), \\ (q \cdot \epsilon_i)(q \cdot \epsilon_j)(q \cdot \epsilon_k)(q \cdot \epsilon_l) & \mapsto \frac{1}{(d-1)^2} \bar{q}^4 (\epsilon_i \cdot \epsilon_j)(\epsilon_k \cdot \epsilon_l), \end{aligned}$$

together with Table V.

TABLE V: The values of the products of polarization vectors in the S -wave effective potentials with total angular momentum $J = 0, 1$, and 2 , respectively [57].

Terms	$J = 0$	$J = 1$	$J = 2$
\mathcal{O}_1	1	1	1
\mathcal{O}_2	1	-1	1
\mathcal{O}_3	3	0	0

IV. NUMERICAL RESULTS AND DISCUSSIONS

A. Potentials in coordinate space and possible bound states

After obtaining the scattering amplitudes, we now evaluate the effective potentials and analyze their behaviors in coordinate space. To obtain the numerical results, we use the following LECs, determined by the resonance saturation model [55, 57, 58]:

$$D_a = -13.23 \text{ GeV}^{-2}, E_a = -11.49 \text{ GeV}^{-2}. \quad (99)$$

Other parameters include: $m_\pi = 0.139 \text{ GeV}$, the pion decay constant $f_\pi = 0.086 \text{ GeV}$, the renormalization scale $\mu = 4\pi f_\pi$, $\delta_1 = 0.142 \text{ GeV}$, $\delta_2 = 0.045 \text{ GeV}$, and the coupling constants $g_1 = 0.065$ and $g_2 = 0.52$ [57].

Then we will substitute the potentials into the Schrödinger equation and search for the bound states. In this work, we regularize the effective potentials using the Gauss regulator $\mathcal{F}(\mathbf{q}) = \exp(-\mathbf{q}^{2n}/\Lambda^{2n})$ to prevent the divergence at high momentum transfer. Usually, the value of the cutoff parameter Λ in chiral effective field theory is around 0.5 GeV [53, 59, 62].

TABLE VI: The coefficients appearing in the contact term amplitudes at NLO (Eqs.(57)-(74)).

	$I = 1$			$I = 0$			ω_1	ω_2
	A_1	A_2	A_3	A_1	A_2	A_3		
$A_{a3.1}$	$\frac{1}{4}(3D_a - E_a)$	$\frac{1}{4}(3D_b - E_b)$	$\frac{1}{4}(3D_b - E_b)$	$\frac{3}{4}(D_b + E_b)$	$\frac{3}{4}(D_b + E_b)$	$\frac{3}{4}(D_b + E_b)$	0	0
$A_{a3.2}$	$\frac{1}{4}(3D_a - E_a)$	0	0	$\frac{3}{4}(D_a + E_a)$	0	0	δ_2	δ_2
$A_{a3.3(4)}$	$\frac{1}{4}(3D_a - E_a)$	$\frac{1}{4}(3D_a - E_a)$	0	$\frac{3}{4}(D_b + E_b)$	$\frac{3}{4}(D_b + E_b)$	0	$0(\delta_2)$	$\delta_2(0)$
$A_{a3.5}$	0	0	0	0	0	0	0	0
$A_{a3.6}$	0	0	0	0	0	0	δ_1	δ_1
$A_{a3.7(8)}$	0	0	0	0	0	0	$0(\delta_1)$	$\delta_1(0)$
$A_{a3.9}$	$\frac{1}{4}(D_b + E_b)$	$\frac{1}{4}(D_a + E_a)$	$\frac{1}{4}[\frac{(d-3)(D_b + E_b)}{(D_a + E_a)}]$	$\frac{-3}{4}(D_b - 3E_b)$	$\frac{-3}{4}(D_b - 3E_b)$	$\frac{-3}{4}[\frac{(d-3)(D_b - 3E_b)}{(D_a - 3E_a)}]$	0	0
$A_{a3.10}$	$\frac{1}{4}(D_b + E_b)$	0	0	$\frac{-3}{4}(D_b - 3E_b)$	0	0	δ_1	δ_2
$A_{a3.11(12)}$	$\frac{1}{4}(D_b + E_b)$	$\frac{1}{4}(D_b + E_b)$	0	$\frac{-3}{4}(D_b - 3E_b)$	$\frac{-3}{4}(D_b - 3E_b)$	0	$0(\delta_1)$	$\delta_2(0)$
$A_{a3.13}$	$\frac{1}{4}(D_b + E_b)$	$\frac{1}{4}(D_a + E_a)$	$\frac{1}{4}[\frac{(d-3)(D_b + E_b)}{(D_a + E_a)}]$	$\frac{-3}{4}(D_b - 3E_b)$	$\frac{-3}{4}(D_b - 3E_b)$	$\frac{-3}{4}[\frac{(d-3)(D_b - 3E_b)}{(D_a - 3E_a)}]$	0	0
$A_{a3.14}$	$\frac{1}{4}(D_b + E_b)$	0	0	$\frac{-3}{4}(D_b - 3E_b)$	0	0	δ_1	δ_2
$A_{a3.15(16)}$	$\frac{1}{4}(D_b + E_b)$	$\frac{1}{4}(D_b + E_b)$	0	$\frac{-3}{4}(D_b - 3E_b)$	$\frac{-3}{4}(D_b - 3E_b)$	0	$0(\delta_1)$	$\delta_2(0)$
$A_{a3.(17+18)}$	$D_a + E_a$	$D_b + E_b$	$D_b + E_b$	$D_a - 3E_a$	$D_b - 3E_b$	$D_b - 3E_b$	0	δ_2
$A_{a3.(19+20)}$	$D_a + E_a$	$D_b + E_b$	$D_b + E_b$	$D_a - 3E_a$	$D_b - 3E_b$	$D_b - 3E_b$	0	δ_1

TABLE VII: The constants A (as well as $\omega_{1,2}$) appearing in the OPE amplitudes (Eqs. (75)-(86)).

	$A_{b3.1}$	$A_{b3.2(3)}$	$A_{b3.4}$	$A_{b3.5(6)}$	$A_{b3.7}$	$A_{b3.8}$	$A_{b3.9}$	$A_{b3.(10+11)}$	$A_{b3.(12+13)}$	$A_{b3.14(15)}$	$A_{b3.16(17)}$
$I = 1$	$-\frac{1}{16}$	$-\frac{1}{16}$	$-\frac{1}{16}$	$-\frac{1}{16}$	$-\frac{1}{12}$	$-\frac{1}{12}$	$\frac{1}{4}$	$\frac{1}{4}$	$\frac{1}{4}$	0	0
$I = 0$	$\frac{3}{16}$	$\frac{3}{16}$	$\frac{3}{16}$	$\frac{3}{16}$	$\frac{1}{4}$	$\frac{1}{4}$	$-\frac{3}{4}$	$-\frac{3}{4}$	$-\frac{3}{4}$	0	0
ω_1	0	$\delta_2(0)$	0	$0(\delta_1)$	0	0	0	0	0	0	0
ω_2	0	$0(\delta_2)$	0	$\delta_1(0)$	0	0	0	δ_1	δ_2	0	0

1. $D\bar{B}$ systems

Firstly, we analyze the behaviors of the effective potentials of the $D\bar{B}$ systems, which receive contributions from the contact and the TPE terms. There are two channels: $I(J^P) = 1(0^+)$ and $I(J^P) = 0(0^+)$, and their effective potentials in coordinate space are shown in Figs. 4(a) and 4(b), respectively. Here, we adopt the cutoff parameter Λ with 0.5 GeV.

For the $I(J^P) = 1(0^+)$ state in Fig. 4(a), we observe that although attractive, the TPE interaction is much weaker than the repulsive contact interaction, resulting

in an overall repulsive potential. Accordingly, no bound states are found in this system.

For the $I(J^P) = 0(0^+)$ system, the effective potentials are shown in Fig. 4(b). Compared to the $I(J^P) = 1(0^+)$ system, we can find that the TPE potential is weakly repulsive, while the contact potential is attractive. However, the summed attraction is too weak, so no bound state is found in this system.

It is worth noting that the effective potentials of the $I(J^P) = 1(0^+)$ $D\bar{B}$ system have similar behaviors with the potentials of the $I(J^P) = 1(0^+)$ $\bar{B}\bar{B}$ system in Ref. [57], which is a consequence of heavy flavor symme-

TABLE VIII: The constants appearing in the TPE amplitudes (Eqs. (87)-(98)). Note that we have $A_{51} = A_{15}$.

	$I = 1$			$I = 0$			ω_1	ω_2
	A_1	A_5	A_{15}	A_1	A_5	A_{15}		
$A_{c3.1}$	$\frac{1}{16}$	$\frac{1}{16}$	$-\frac{1}{16}$	$-\frac{3}{16}$	$-\frac{3}{16}$	$\frac{3}{16}$	0	0
$A_{c3.2}$	$\frac{i}{8}$	$-\frac{i}{8}$	0	$-\frac{3i}{8}$	$\frac{3i}{8}$	0	δ_2	0
$A_{c3.3}$	$\frac{i}{8}$	$-\frac{i}{8}$	0	$-\frac{3i}{8}$	$\frac{3i}{8}$	0	0	0
$A_{c3.4}$	$\frac{i}{8}$	$-\frac{i}{8}$	0	$-\frac{3i}{8}$	$\frac{3i}{8}$	0	δ_1	0
$A_{c3.5}$	$\frac{i}{8}$	$-\frac{i}{8}$	0	$-\frac{3i}{8}$	$\frac{3i}{8}$	0	0	0
$A_{c3.6}$	$\frac{1}{16}$	0	0	$\frac{9}{16}$	0	0	δ_1	δ_2
$A_{c3.7}$	$\frac{1}{16}$	0	0	$\frac{9}{16}$	0	0	0	0
$A_{c3.8}$	$\frac{1}{16}$	0	0	$\frac{9}{16}$	0	0	δ_1	0
$A_{c3.9}$	$\frac{1}{16}$	0	0	$\frac{9}{16}$	0	0	0	δ_2
$A_{c3.10}$	$\frac{5}{16}$	0	0	$-\frac{3}{16}$	0	0	δ_1	δ_2
$A_{c3.11}$	$\frac{5}{16}$	0	0	$-\frac{3}{16}$	0	0	0	0
$A_{c3.12}$	$\frac{5}{16}$	0	0	$-\frac{3}{16}$	0	0	δ_1	0
$A_{c3.13}$	$\frac{5}{16}$	0	0	$-\frac{3}{16}$	0	0	0	δ_2

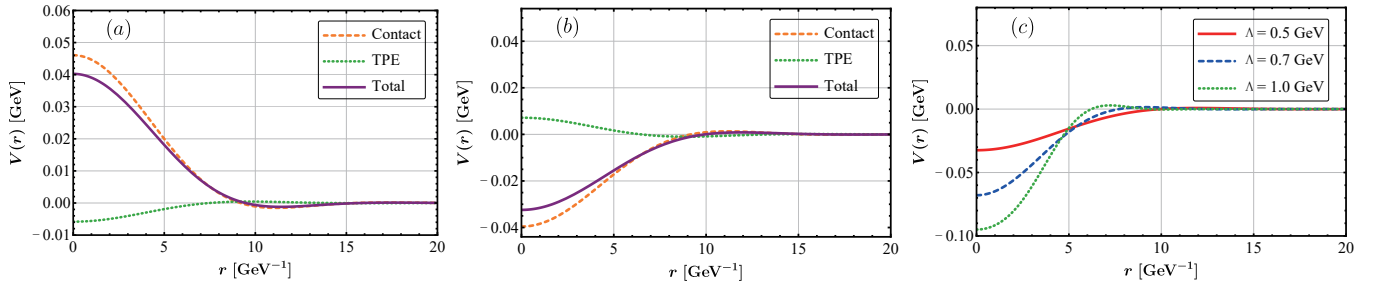


FIG. 4: S -wave potential of the $D\bar{B}$ systems and the dependence of the total potential on the cutoff parameter, namely, (a) the potential of $I(J^P) = 1(0^+)$ $D\bar{B}$ system at $\Lambda = 0.5$ GeV, (b) the potential of $I(J^P) = 0(0^+)$ $D\bar{B}$ system at $\Lambda = 0.5$ GeV, (c) the total potential of $D\bar{B}[1(0^+)]$ system with different cutoffs. The green dashed, red dashed lines, and purple solid lines represent the contact, TPE, and full potential, respectively.

try between the charm and bottom quarks. As shown in Fig. 4(c), the total potentials become more and more attractive as the cutoff parameter Λ increases. The bound states emerge at $\Lambda = 0.7$ GeV and $\Lambda = 1.0$ GeV, lying 0.8 MeV and 3.6 MeV below the $D\bar{B}$ mass threshold, respectively. However, we change the cutoff to 0.54 GeV, the very shallow bound state can emerge in the $D\bar{B}[0(0^+)]$ channel.

2. $D\bar{B}^*$ systems

In this section, we investigate the interactions of the $D\bar{B}^*$ systems with $I(J^P) = 1(1^+)$ and $I(J^P) = 0(1^+)$. As shown in Fig. 2 before, only the contact diagram contributes to the amplitudes at LO. The one-loop corrections to the contact diagrams and TPE diagrams appear at NLO. Their results are shown in Figs. 5(a) and 5(b) we adopt the cutoff parameter Λ with 0.5 GeV.

Comparing Fig. 5(a) with Fig. 4(a), we observe that the behavior of the $D\bar{B}^*[1(1^+)]$ effective potential is sim-

ilar with the $D\bar{B}[1(0^+)]$ effective potential. For the $D\bar{B}^*[1(1^+)]$ system, the repulsive contact interaction is much stronger than the attractive TPE interaction, which leads to a net repulsive potential. As a result, no bound state exists in this system.

In the case of the $D\bar{B}^*[0(1^+)]$ system, the effective potentials are shown in Fig. 5(b). Compared to the $1(1^+)$ system, the behaviors of the $0(1^+)$ contact and TPE potential are both reversed, which results in an overall attractive interaction. However, this potential is weaker even than the one in the previous $D\bar{B}[0(0^+)]$ system. As shown in Fig. 5(c), the total potential at $\Lambda = 0.7$ GeV and at $\Lambda = 0.5$ GeV are of similar strength. However, when $\Lambda = 1.0$ GeV, the effective potential is repulsive near the origin but becomes attractive at intermediate distances. This behavior appears because the TPE contribution at large momentum is more sensitive to cutoff Λ variations, which leads to a repulsive potential at short distances. In our calculation, no bound state is found in the $D\bar{B}^*[0(1^+)]$ system.

Therefore we conclude that the interaction in the $D\bar{B}^*[0(1^+)]$ system is weaker than that in the $D\bar{B}[0(0^+)]$ system. This is consistent with the predictions of the one-boson-exchange potential model [34], but contrasts with the conclusions drawn from lattice QCD calculations [49].

3. $D^*\bar{B}^*$ systems

In this section, we explore the possibility of bound states in the $D^*\bar{B}^*$ systems, which includes six different isospin-spin states: $1(0^+)$, $0(0^+)$, $1(1^+)$, $0(1^+)$, $1(2^+)$, and $0(2^+)$. At LO, both contact and OPE contribute to the effective potential. At NLO, the one-loop corrections to the contact and OPE diagrams shown in Fig. 3 as well as TPE diagrams all contribute.

First, we focus on the $J^P = 0^+ D^*\bar{B}^*$ state. The effective potentials are shown in Figs. 6(a) and 6(b), we adopt the cutoff parameter Λ with 0.5 GeV. In Fig. 6(a), we observe that both the contact and OPE interactions are repulsive, while the TPE interaction is attractive. However, the total potential is repulsive, meaning no bound state can exist in the $1(0^+)$ $D^*\bar{B}^*$ system. In contrast, for the $0(0^+)$ system in Fig. 6(b), the contact and OPE interactions provide an attractive force, while the TPE interaction is repulsive. The repulsive TPE contribution partially counteracts the attractive contact interaction, but the OPE interaction remains strong enough to form a bound state. The resulting binding energy is $\Delta E = 6.0$ MeV. As shown in Fig. 6, the OPE terms can contribute to the total interaction of $D^*\bar{B}^*$ systems, it is a departure from the $D\bar{B}^{(*)}$ systems.

The Λ dependence of the $I(J^P) = 0(0^+)$ total potential is shown in Fig. 6(c). We find that the total interaction is sensitive to the cutoff, particularly near the origin, which stems from the TPE contribution. As the cutoff increases to 1.0 GeV, the binding energy becomes 35.9 MeV.

Next, we analyze the interactions in the $D^*\bar{B}^*[1^+]$

system. For the $1(1^+)$ state, as seen in Fig. 7(a), the OPE contribution is largely offset by the TPE contribution, with the repulsive contact potential remaining. It results in a fully repulsive total potential, meaning no bound state exists in the $D^*\bar{B}^*[1(1^+)]$ system. For the $D^*\bar{B}^*[0(1^+)]$ system, the effective potentials, shown in Fig. 7(b), exhibit similar behaviors to those of the $D^*\bar{B}^*[0(0^+)]$ system. Although the attraction is not as strong as in the $D^*\bar{B}^*[0(0^+)]$, it is still sufficient to form a shallow bound state. By solving the Schrödinger equation, we obtain the $D^*\bar{B}^*[0(1^+)]$ binding energy $\Delta E = 0.6$ MeV at $\Lambda = 0.5$ GeV.

Finally, we examine the possibility of bound state formations in the $J^P = 2^+ D^*\bar{B}^*$ system. In Fig. 8(a), for the $1(2^+)$ $D^*\bar{B}^*$ system, both the OPE and TPE potentials are mildly attractive, while the dominant contact potential remains repulsive, resulting in a repulsive total potential.

We also calculate the effective potentials for the $D^*\bar{B}^*[0(2^+)]$ system, with the potential profiles shown in Fig. 8(b). In this situation, both the OPE and TPE act as repulsive forces that counter the attractive force from the contact term, leading to an overall repulsive potential. This behavior contrasts with the attractive effective potential of the other $D^{(*)}\bar{B}^{(*)}$ systems with $I = 0$. Consequently, there is no evident bound state in the $D^*\bar{B}^*[0(2^+)]$ system.

Similarly, the effective potentials of $D^*\bar{B}^*[0(2^+)]$ at different cutoff parameters are shown in Fig. 8(c). Although the total interaction is repulsive at small distances, as seen in other channels, the potential becomes attractive in the intermediate range at $\Lambda = 1.0$ GeV. This attraction allows the $D^*\bar{B}^*$ mesons to form a bound state, which lies 4.3 MeV below the threshold.

Based on the above calculations and analyses, we have obtained the coordinate potentials and determined the possible bound states by solving the Schrödinger equation. The total interactions are repulsive in the $I = 1$ channels and attractive in the $I = 0$ channels. Then, we focus on the $I = 0$ $D^{(*)}\bar{B}^{(*)}$ systems to search for bound states. For the $D\bar{B}[0(0^+)]$, $D\bar{B}^*[0(1^+)]$, and $D^*\bar{B}^*[0(2^+)]$ systems, the attractive potentials are too weak to bind the mesons, and no definite bound states are found in these channels at a cutoff of $\Lambda = 0.5$ GeV. However, if we change the cutoff to 0.54 GeV, the very shallow bound state can emerge in the $D\bar{B}[0(0^+)]$ channel. As for the $D\bar{B}^*[0(1^+)]$, the bound state appears at $\Lambda = 1.02$ GeV, and the binding energy will increase as the Λ get larger.

Besides, in the $D^*\bar{B}^*[0(0^+)]$ and $D^*\bar{B}^*[0(1^+)]$ channels, two shallow bound states are found with binding energies of 6.0 MeV and 0.6 MeV, respectively. Therefore, we suggest that future theoretical and experimental studies should focus on these two systems to find new heavy tetraquark states. Compared the total potentials of the five $I = 0$ channels, we can also conclude that the interaction in $D^*\bar{B}^*[0(0^+)]$ channel is more attractive than the other four channels. The mass and the binding

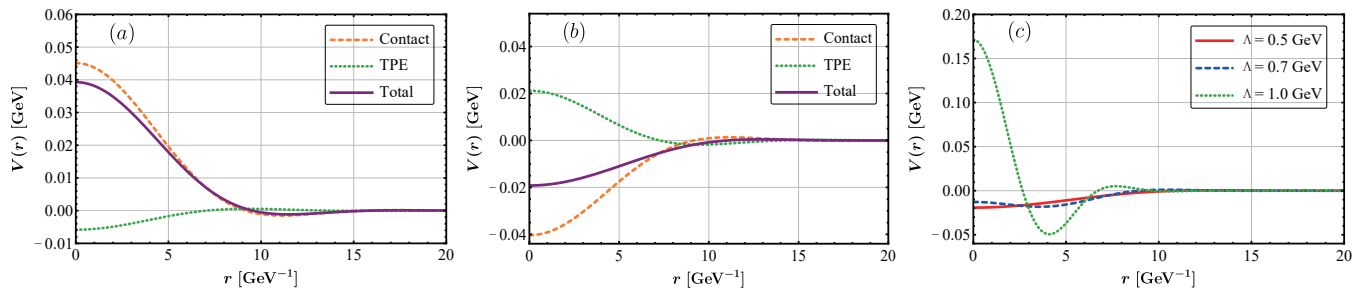


FIG. 5: S -wave potential of the $D\bar{B}^*$ systems and the dependence of the total potential on the cutoff parameter, namely, (a) the potential of $I(J^P) = 1(1^+)$ $D\bar{B}^*$ system at $\Lambda = 0.5$ GeV, (b) the potential of $I(J^P) = 0(1^+)$ $D\bar{B}^*$ system at $\Lambda = 0.5$ GeV, (c) the total potential of $D\bar{B}^*[0(1^+)]$ system with different cutoffs. The green dashed and red dashed lines represent the contact and TPE contributions, respectively. The purple solid lines stand for the full potential.

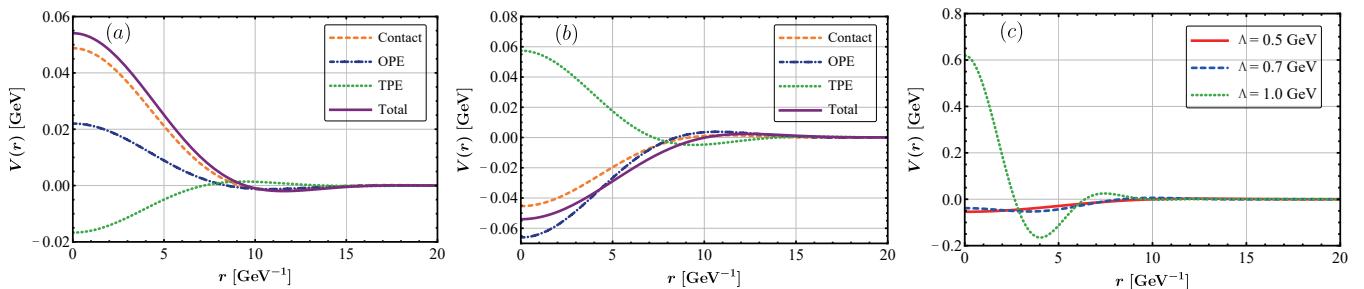


FIG. 6: S -wave potential of $J = 0$ $D^*\bar{B}^*$ systems and the dependence of the total potential on the cutoff parameter, namely, (a) the potential of $I(J^P) = 1(0^+)$ $D^*\bar{B}^*$ system at $\Lambda = 0.5$ GeV, (b) the potential of $I(J^P) = 0(0^+)$ $D^*\bar{B}^*$ system at $\Lambda = 0.5$ GeV, (c) the total potential of $D^*\bar{B}^*[0(0^+)]$ system with different cutoffs. The green dashed, blue dashed, and red dashed lines represent the contact, OPE, and TPE contributions, respectively. The purple solid lines stand for the full potential.

energy of each $D^{(*)}\bar{B}^{(*)}[I = 0]$ system under different cutoffs are listed in Table IX.

B. Two-body scattering of $D^{(*)}\bar{B}^{(*)}$ systems

In addition to the binding energies, we further derive information about $D^{(*)}\bar{B}^{(*)}$ elastic scattering by solving the Lippmann-Schwinger equation. In quantum theory, the scattering rate represents the probability per unit time for a scattering event, it is proportional to the cross section, the number of the targets, and the flux [63]. Using Eqs. (12)-(16), we now calculate the scattering rates between $D^{(*)}$ and $\bar{B}^{(*)}$. The variations of the scattering rates $k\sigma(k)$ with cutoffs are shown in Figs. 9 and 10, as functions of the center-of-mass energy.

The scattering length and effective range can be related to the interaction between particles through the scattering amplitude or phase shift [65]. Based on Eq. (15), we also evaluate the scattering lengths and effective ranges at different cutoff values Λ , with numerical results listed in Table X.

Let us focus on the scattering rates $k\sigma(k)$ for the $D\bar{B}^*[0(0^+)]$ and $D\bar{B}^*[0(1^+)]$ systems in Figs. 9(a) and 9(b). The enhancement of $k\sigma(k)$ near the threshold is gradual, which is insufficient to confirm the presence of a bound or virtual state. Look at the scattering lengths and effective ranges in Table X, We find that the scattering lengths a for different cutoffs are negative, which indicates that the phase shifts satisfy $0 \leq \delta < \pi/2$ [64]. As a result, there are no evident bound states in the two systems, which aligns with the outcomes found in the previous subsection by solving the Schrödinger equation.

We now move to the scattering of the two vector meson systems. The scattering rates for the $D^*\bar{B}^*[0(0^+)]$, $D^*\bar{B}^*[0(1^+)]$, and $D^*\bar{B}^*[0(2^+)]$ systems are shown in Fig. 10. Near the thresholds, there are significant enhancements, which may indicate the presence of possible bound or virtual states.

In Table X, we find that, in the $D^*\bar{B}^*[0(0^+)]$ system, the scattering lengths are positive for different cutoff values, indicating the presence of unambiguous bound states, which supports the calculations in above subsection.

For the $D^*\bar{B}^*[0(1^+)]$ system, the scattering length is negative at $\Lambda = 0.5$ GeV and $\Lambda = 0.7$ GeV, but it takes

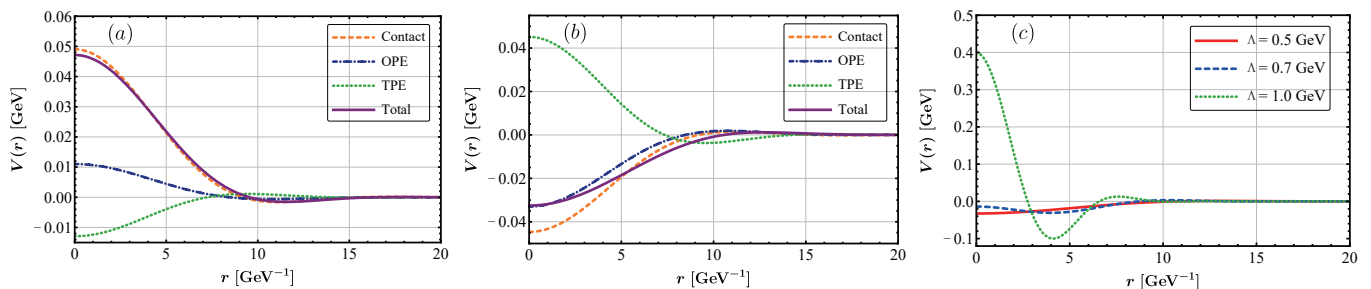


FIG. 7: S -wave potential of $J = 1$ $D^* \bar{B}^*$ systems and the dependence of the total potential on the cutoff parameter, namely, (a) the potential of $I(J^P) = 1(1^+)$ $D^* \bar{B}^*$ system at $\Lambda = 0.5$ GeV, (b) the potential of $I(J^P) = 0(1^+)$ $D^* \bar{B}^*$ system at $\Lambda = 0.5$ GeV, (c) the total potential of $D^* \bar{B}^*[0(1^+)]$ system on the different cutoffs. The green dashed, blue dashed, and red dashed lines represent the contact, OPE, and TPE contributions, respectively. The purple solid lines stand for the full potential.

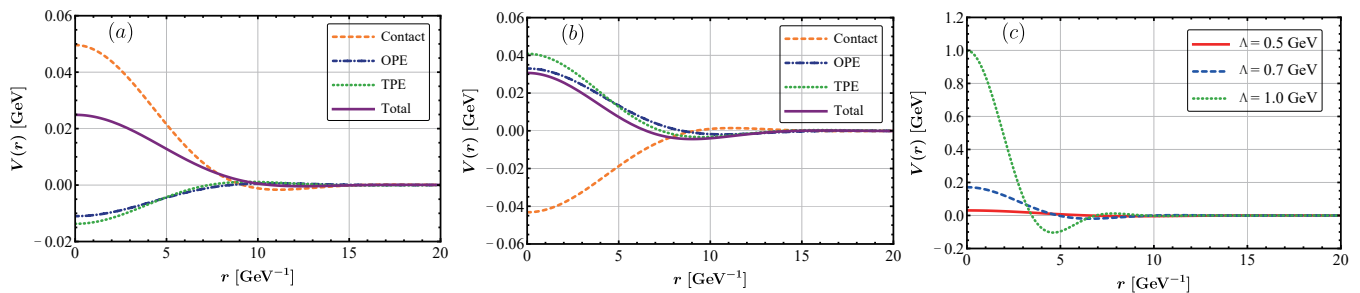


FIG. 8: S -wave potential of $J = 2$ $D^* \bar{B}^*$ systems and the dependence of the total potential on the cutoff parameter, namely, (a) the potential of $I(J^P) = 1(2^+)$ $D^* \bar{B}^*$ system at $\Lambda = 0.5$ GeV, (b) the potential of $I(J^P) = 0(2^+)$ $D^* \bar{B}^*$ system at $\Lambda = 0.5$ GeV, (c) the total potential of $D^* \bar{B}^*[0(2^+)]$ system with the different cutoffs. The green dashed, blue dashed, and red dashed lines represent the contact, OPE, and TPE contributions, respectively. The purple solid lines stand for the full potential.

on a large positive value at $\Lambda = 1.0$ GeV, signaling the existence of a shallow bound state.

Additionally, we evaluate the corresponding phase shifts for these S -wave bound systems according to Eq. (14). We find that

$$\lim_{k \rightarrow 0} \delta_0 = \pi, \quad (100)$$

which is consistent with Levinson's theorem [65], describing the physical connection between phase shifts and the existence of bound states.

For the $D^* \bar{B}^*[0(2^+)]$ system at different cutoffs, the effective interaction is attractive at small momentum (large distance) but repulsive at large momentum (small distance). It initially causes a positive phase shift at low momentum and then a negative phase shift at high momentum, so that the scattering rate drops to zero, and then gradually increases against the center-of-momentum energy. The negative scattering length indicates that the attractive effect is not strong enough to bind D^* and \bar{B}^* together in $0(2^+)$ channel.

C. Estimation of the contact term LECs

For the $D\bar{B}[0(0^+)]$ and $D\bar{B}^*[0(1^+)]$ systems, the above calculations show that the total potentials are not strong enough to form bound states for the heavy mesons. However, this does not imply that no bound state can exist in these systems. Note that the contact terms are determined using the resonance saturation model, therefore, we now explore alternative methods to redetermine the LECs of the contact terms in this work.

Recently, a lattice QCD study conducted by Alexandrou *et al.* [49] found shallow bound states for both $J = 0$ and $J = 1$ $\bar{b}cud$ tetraquarks, with binding energies of $0.5^{+0.4}_{-1.5}$ MeV and $2.4^{+2.0}_{-0.7}$ MeV, respectively. Padmanath *et al.* reported a lattice QCD research indicating that an $I(J^P) = 0(1^+)$ $\bar{b}cud$ bound state with a binding energy of $43^{(+7)}_{(-6)} \binom{+24}{-14}$ MeV can exist below the $B^* \bar{D}$ threshold [50]. And, they presented another study searching for tetraquark candidates with exotic quark content $bc\bar{u}\bar{d}$ in the $I = 0$ and $J^P = 0^+$ channel, and found a sub-threshold pole in the S -wave $D\bar{B}$ scattering amplitude, which corresponds to the binding energy of $39^{(+4)}_{(-6)} \binom{+8}{-18}$ MeV below the $D\bar{B}$ threshold [51]. The above results provide valuable references for redetermining

TABLE IX: The bound states in the five $D^{(*)}\bar{B}^{(*)}$ systems with $I = 0$. The cutoff parameter Λ , state mass M , and binding energy E are in units of GeV, MeV, and MeV respectively. “...” means that there is no bound state.

Λ	$D\bar{B}$		$D\bar{B}^*$		$D^*\bar{B}^*(J=0)$		$D^*\bar{B}^*(J=1)$		$D^*\bar{B}^*(J=2)$	
	M	E	M	E	M	E	M	E	M	E
0.5	7235.7	6.0	7241.1	0.6
0.7	7143.6	0.8	7230.6	11.1	7240.0	1.7
1.0	7140.8	3.6	7205.8	35.9	7232.3	9.4	7237.4	4.3

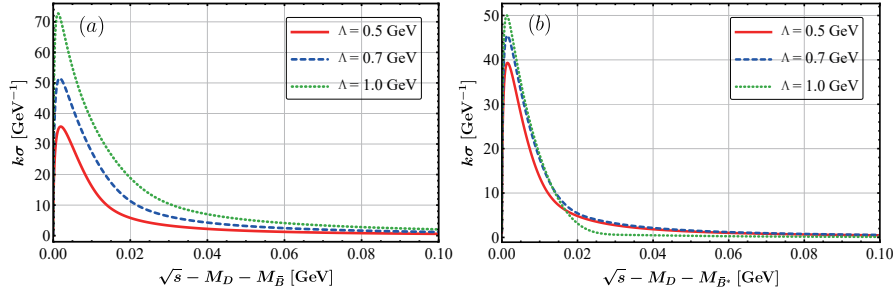


FIG. 9: The dependencies of the S -wave scattering rates for the $D\bar{B}[0(0^+)]$ system and $D\bar{B}^*[0(1^+)]$ system on the cutoff Λ .

ing the contact terms’ LECs.

To ascertain the possible parameter region which allows bound states exist in the $D\bar{B}[0(0^+)]$ and $D\bar{B}^*[0(1^+)]$ systems at $\Lambda = 0.5$ GeV, we can vary the LECs D_a and E_a within the ranges $[-80, 10]$ GeV^{-2} and $[-50, -10]$ GeV^{-2} , respectively. We find that when the LECs satisfy the relation:

$$D_a - 3E_a = 22.2 \text{ GeV}^{-2}, \quad (101)$$

a bound state forms with almost zero binding energy. When the LECs satisfy

$$D_a - 3E_a = 69.0 \text{ GeV}^{-2}, \quad (102)$$

a bound state with a binding energy of 30 MeV below the $D\bar{B}$ threshold can be obtained. The green band in Fig. 11 represents the corresponding parameter region. Similarly, we can also determine the contact term LECs for the $D\bar{B}^*[0(1^+)]$ system. For binding energy of 0 MeV, we have:

$$D_a - 3E_a = 27.3 \text{ GeV}^{-2}, \quad (103)$$

and for a binding energy of 30 MeV:

$$D_a - 3E_a = 72.6 \text{ GeV}^{-2}. \quad (104)$$

The corresponding parameter variations are shown as the purple band in Fig. 11. The arrow indicates the direction in which the binding energy increases for both the $D\bar{B}[0(0^+)]$ and $D\bar{B}^*[0(1^+)]$ systems.

Notably, in this analysis, the attraction between D and \bar{B} is stronger than that between D and \bar{B}^* . This contrasts the results reported in Ref. [49] but is consistent with the results obtained using the one-boson-exchange model [34].

V. SUMMARY

In this work, we systematically investigate the interactions of the S -wave $D^{(*)}\bar{B}^{(*)}$ systems within the framework of ChEFT using the heavy hadron formalism. We calculate the effective potentials, including contributions from the contact, OPE, and TPE terms, up to NLO at the one-loop level, adopting Weinberg’s formalism. By performing a Fourier transformation, we analyze the behaviors of the effective potentials in coordinate space in detail and employ the Gauss form factor to regularize the divergence in the integral at large momentum. We then insert the coordinate space potentials into the Schrödinger equation to search for potential $D^{(*)}\bar{B}^{(*)}$ bound states.

The results show that all total potentials in the $I = 1$ channels are repulsive, whereas those in the $I = 0$ channels are attractive. Further calculations examine the variation of interactions with the cutoff parameter Λ across five $I = 0$ $D^{(*)}\bar{B}^{(*)}$ channels. We find that bound states are more likely to exist in the $D\bar{B}[0(0^+)]$, $D^*\bar{B}^*[0(0^+)]$, and $D^*\bar{B}^*[0(1^+)]$ channels. Notably, the TPE contributions are more sensitive to the cutoff in the $I = 0$ $D^*\bar{B}^*$ channels and play a dominant role in these

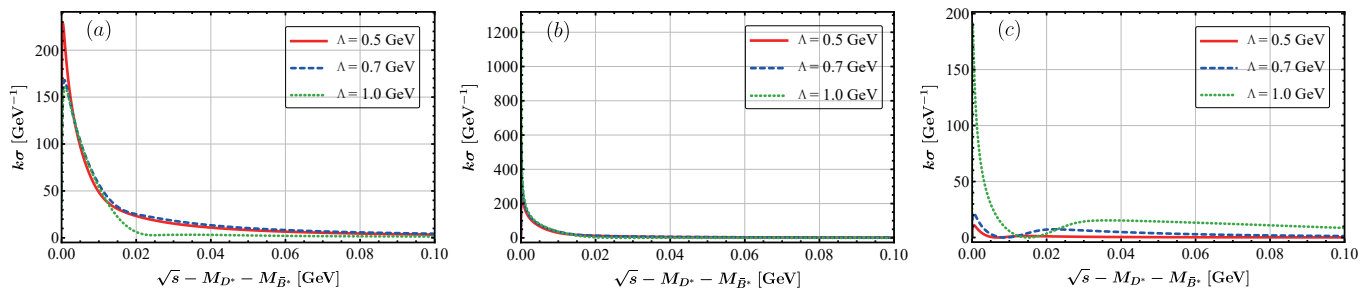


FIG. 10: The dependence of the S -wave scattering rate $k\sigma$ for the $D^*\bar{B}^*[0(0^+)]$, $D^*\bar{B}^*[0(1^+)]$, $D^*\bar{B}^*[0(2^+)]$ systems on the cutoff Λ .

TABLE X: The scattering length a and effective range r in the five $D^{(*)}\bar{B}^{(*)}[I=0]$ scattering channels. The cutoff parameter Λ , a , and r are in units of GeV, fm, and fm respectively.

Λ	$D\bar{B}$		$D\bar{B}^*$		$D^*\bar{B}^*(J=0)$		$D^*\bar{B}^*(J=1)$		$D^*\bar{B}^*(J=2)$	
	a	r	a	r	a	r	a	r	a	r
0.5	-1.64	2.60	-1.86	2.05	6.37	1.91	-9.87	0.54	-1.25	11.05
0.7	-2.12	2.21	-2.03	1.97	4.48	1.97	-24.06	0.71	-1.76	7.97
1.0	-2.74	1.85	-2.22	2.08	4.38	0.92	140.94	1.19	-7.31	3.67

channels, unlike the case in $D\bar{B}[0(0^+)]$. We list the mass and binding energies in Table IX.

By substituting the momentum space potentials into the Lippmann-Schwinger equation, we calculate the scattering T -matrices and the associated scattering phase shifts. To gain further insight into the S -wave $D^{(*)}\bar{B}^{(*)}$ interactions, we calculate the scattering rate, scattering length, and effective range, and provide their numerical results in Table X based on the T -matrix and scattering phase. Accordingly, we study the dependence of these physical quantities on the cutoff parameter Λ . In our investigation, the shallow bound state is more likely to exist in the $D\bar{B}[I(J^P) = 0(0^+)]$ system than in the $D\bar{B}^*[I(J^P) = 0(1^+)]$ system.

Based on the above calculations, we find that the interactions in the $D^*\bar{B}^*[I=0]$ system are more attractive than those in the $D\bar{B}^{(*)}[I=0]$ systems, and $D^*\bar{B}^*[I(J^P) = 0(0^+)]$ and $D^*\bar{B}^*[I(J^P) = 0(1^+)]$ systems possess large binding energies and positive scattering lengths, which suggests strong bound state formations in these channels. Therefore, we strongly recommend the experiment to find the $D^*\bar{B}^*[I=0]$ tetraquark systems.

Considering other theoretical and lattice QCD studies,

we redetermined the contact term LECs and calculated the effective potentials for the $0(0^+)$ $D\bar{B}$ system and the $0(1^+)$ $D\bar{B}^*$ system. In Fig. 11, we present the dependencies of the binding energies of these two charm-bottom systems on the redetermined contact LECs D_a and E_a .

Building on our calculations and analysis, we can comprehensively compare previous theoretical and lattice QCD studies. Our results provide valuable insights to inform future experimental research.

ACKNOWLEDGMENTS

Zhe Liu expresses sincere gratitude to Prof. Zhan-Wei Liu for their insightful discussions and extends thanks to Zi-Le Zhang and Ri-Qing Qian for their valuable contributions to the discussions. This work is supported by the National Natural Science Foundation of China under Grant Nos. 12335001, 12247101, 12465016 and 12005168, the ‘‘111 Center’’ under Grant No. B20063, the Natural Science Foundation of Gansu Province (No. 22JR5RA389 and No. 22JR5RA171), the fundamental Research Funds for the Central Universities (Grant No. lzujbky-2023-stlt01), and the project for top-notch innovative talents of Gansu province.

[1] R. Aaij *et al.* [LHCb], A model-independent study of resonant structure in $B^+ \rightarrow D^+ D^- K^+$ decays, Phys. Rev. Lett. **125**, 242001 (2020).

[2] R. Aaij *et al.* [LHCb], Amplitude analysis of the $B^+ \rightarrow D^+ D^- K^+$ decay, Phys. Rev. D **102**, 112003 (2020).

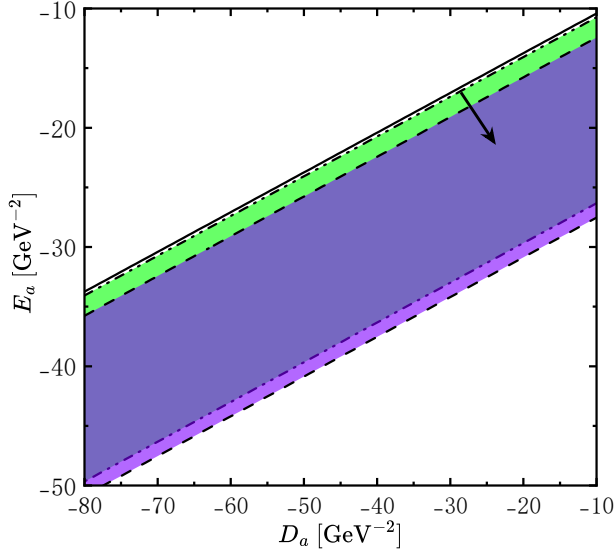


FIG. 11: The binding energies of the $D\bar{B}[0(0^+)]$ and $D\bar{B}^*[0(1^+)]$ states vary with the redetermined contact LECs D_a and E_a with cutoff $\Lambda = 0.5$ GeV. The purple and green bands correspond to the $D\bar{B}$ and $D\bar{B}^*$ systems, respectively. The black solid line represents the contact LECs determined by the resonance saturation model. The parallel dashed (dotted) lines at the boundaries of the purple (green) band stand for the regions of parameters within the binding energies 0 MeV and 30 MeV. The arrow stands for the direction that binding energy increases for both $D\bar{B}[0(0^+)]$ and $D\bar{B}^*[0(1^+)]$ systems.

- [3] R. Aaij *et al.* [LHCb], Observation of an exotic narrow doubly charmed tetraquark, *Nature Phys.* **18**, 751-754 (2022).
- [4] R. Aaij *et al.* [LHCb], Study of the doubly charmed tetraquark T_{cc}^+ , *Nature Commun.* **13**, 3351 (2022).
- [5] R. Aaij *et al.* [LHCb], First Observation of a Doubly Charged Tetraquark and Its Neutral Partner, *Phys. Rev. Lett.* **131**, 041902 (2023).
- [6] R. Aaij *et al.* [LHCb], Amplitude analysis of $B^+ \rightarrow D^- D_s^+ \pi^+$ and $B^0 \rightarrow \bar{D}^0 D_s^+ \pi^+$ decays, *Phys. Rev. D* **108**, 012017 (2023).
- [7] Y. Cui, X. L. Chen, W. Z. Deng and S. L. Zhu, The Possible Heavy Tetraquarks $qQ\bar{q}\bar{Q}$, $qq\bar{Q}\bar{Q}$ and $qQ\bar{Q}\bar{Q}$, *HEP NP* **31**, 7-13 (2007).
- [8] W. Detmold, K. Orginos and M. J. Savage, BB Potentials in Quenched Lattice QCD, *Phys. Rev. D* **76** (2007), 114503.
- [9] M. V. Carlucci, F. Giannuzzi, G. Nardulli, M. Pellicoro and S. Stramaglia, AdS-QCD quark-antiquark potential, meson spectrum and tetraquarks, *Eur. Phys. J. C* **57**, 569-578 (2008).
- [10] F. S. Navarra, M. Nielsen and S. H. Lee, QCD sum rules study of $QQ - \bar{u}\bar{d}$ mesons, *Phys. Lett. B* **649**, 166-172 (2007).
- [11] Y. Yang, C. Deng, J. Ping and T. Goldman, S -wave $QQ\bar{q}\bar{q}$ state in the constituent quark model, *Phys. Rev. D* **80**, 114023 (2009).
- [12] T. F. Carames, A. Valcarce and J. Vijande, Doubly charmed exotic mesons: A gift of nature?, *Phys. Lett. B* **699**, 291-295 (2011).
- [13] R. Molina, T. Branz and E. Oset, A new interpretation for the $D_{s2}^*(2573)$ and the prediction of novel exotic charmed mesons, *Phys. Rev. D* **82**, 014010 (2010).
- [14] M. L. Du, W. Chen, X. L. Chen and S. L. Zhu, Exotic $QQ\bar{q}\bar{q}$, $QQ\bar{q}\bar{s}$ and $QQ\bar{s}\bar{s}$ states, *Phys. Rev. D* **87**, 014003 (2013).
- [15] T. Hyodo, Y. R. Liu, M. Oka, K. Sudoh and S. Yasui, Production of doubly charmed tetraquarks with exotic color configurations in electron-positron collisions, *Phys. Lett. B* **721**, 56-60 (2013).
- [16] S. Ohkoda, Y. Yamaguchi, S. Yasui, K. Sudoh and A. Hosaka, Exotic mesons with double charm and bottom flavor, *Phys. Rev. D* **86**, 034019 (2012).
- [17] J. Vijande, A. Valcarce and J. M. Richard, Adiabaticity and color mixing in tetraquark spectroscopy, *Phys. Rev. D* **87**, 034040 (2013).
- [18] Y. Ikeda, B. Charron, S. Aoki, T. Doi, T. Hatsuda, T. Inoue, N. Ishii, K. Murano, H. Nemura and K. Sasaki, Charmed tetraquarks T_{cc} and T_{cs} from dynamical lattice QCD simulations, *Phys. Lett. B* **729**, 85-90 (2014).
- [19] P. Bicudo, K. Cichy, A. Peters and M. Wagner, BB interactions with static bottom quarks from Lattice QCD, *Phys. Rev. D* **93**, 034501 (2016).
- [20] P. Bicudo, K. Cichy, A. Peters, B. Wagenbach and M. Wagner, Evidence for the existence of $ud\bar{b}\bar{b}$ and the non-existence of $ss\bar{b}\bar{b}$ and $cc\bar{b}\bar{b}$ tetraquarks from lattice QCD, *Phys. Rev. D* **92**, 014507 (2015).
- [21] A. Peters, P. Bicudo, K. Cichy, B. Wagenbach and M. Wagner, Exploring possibly existing $qq\bar{b}\bar{b}$ tetraquark states with $qq = ud, ss, cc$, *PoS LATTICE2015*, 095 (2016).
- [22] A. Peters, P. Bicudo, L. Leskovec, S. Meinel and M. Wagner, Lattice QCD study of heavy-heavy-light-light tetraquark candidates, *PoS LATTICE2016*, 104 (2016).
- [23] A. Francis, R. J. Hudspith, R. Lewis and K. Maltman, Lattice Prediction for Deeply Bound Doubly Heavy Tetraquarks, *Phys. Rev. Lett.* **118**, 142001 (2017).
- [24] P. Bicudo, M. Cardoso, A. Peters, M. Pflaumer and M. Wagner, $ud\bar{b}\bar{b}$ tetraquark resonances with lattice QCD potentials and the Born-Oppenheimer approximation, *Phys. Rev. D* **96**, 054510 (2017).
- [25] W. Chen, H. X. Chen, X. Liu, T. G. Steele and S. L. Zhu, Open-flavor charm and bottom $sq\bar{q}\bar{Q}$ and $qq\bar{q}\bar{Q}$ tetraquark states, *Phys. Rev. D* **95**, 114005 (2017).
- [26] K. Azizi and U. Özdem, The electromagnetic multipole moments of the charged open-flavor $Z_{\bar{c}q}$ states, *J. Phys. G* **45**, 055003 (2018).
- [27] P. Bicudo, M. Cardoso, A. Peters, M. Pflaumer and M. Wagner, Doubly heavy tetraquark resonances in lattice QCD, *J. Phys. Conf. Ser.* **1137**, 012039 (2019).
- [28] Q. F. Lü, D. Y. Chen and Y. B. Dong, Open charm and bottom tetraquarks in an extended relativized quark model, *Phys. Rev. D* **102**, 074021 (2020).
- [29] X. G. He, W. Wang and R. Zhu, Open-charm tetraquark X_c and open-bottom tetraquark X_b , *Eur. Phys. J. C* **80**, 1026 (2020).
- [30] J. B. Cheng, S. Y. Li, Y. R. Liu, Y. N. Liu, Z. G. Si and T. Yao, Spectrum and rearrangement decays of tetraquark states with four different flavors, *Phys. Rev.*

- D **101**, 114017 (2020).
- [31] R. M. Albuquerque, S. Narison, D. Rabetiarivony and G. Randriamanatrika, $X_{0,1}(2900)$ and $(D^- K^+)$ invariant mass from QCD Laplace sum rules at NLO, Nucl. Phys. A **1007**, 1221 Phys. Rev. D **105**, 054018 13 (2021).
- [32] T. Guo, J. Li, J. Zhao and L. He, Mass spectra and decays of open-heavy tetraquark states, Phys. Rev. D **105**, 054018 (2022).
- [33] H. X. Chen, W. Chen, X. Liu, Y. R. Liu and S. L. Zhu, An updated review of the new hadron states, Rept. Prog. Phys. **86**, 026201 (2023).
- [34] N. Li, Z. F. Sun, X. Liu and S. L. Zhu, Coupled-channel analysis of the possible $D^{(*)}D^{(*)}$, $\bar{B}^{(*)}\bar{B}^{(*)}$ and $D^{(*)}\bar{B}^{(*)}$ molecular states, Phys. Rev. D **88**, 114008 (2013).
- [35] W. Chen, T. G. Steele and S. L. Zhu, Exotic open-flavor $bc\bar{q}\bar{q}$, $bc\bar{s}\bar{s}$ and $qc\bar{q}\bar{b}$, $sc\bar{s}\bar{b}$ tetraquark states, Phys. Rev. D **89**, 054037 (2014).
- [36] S. Q. Luo, K. Chen, X. Liu, Y. R. Liu and S. L. Zhu, Exotic tetraquark states with the $qq\bar{Q}\bar{Q}$ configuration, Eur. Phys. J. C **77**, 709 (2017).
- [37] C. Deng and S. L. Zhu, T_{cc}^+ and its partners, Phys. Rev. D **105**, 054015 (2022).
- [38] W. L. Wu, Y. Ma, Y. K. Chen, L. Meng and S. L. Zhu, Doubly heavy tetraquark bound and resonant states, [arXiv:2409.03373 [hep-ph]].
- [39] E. J. Eichten and C. Quigg, Heavy-quark symmetry implies stable heavy tetraquark mesons $Q_i Q_j \bar{q}_k \bar{q}_l$, Phys. Rev. Lett. **119**, 202002 (2017).
- [40] B. Silvestre-Brac and C. Semay, Systematics of $L = 0$ $q^2\bar{q}^2$ systems, Z. Phys. C **57**, 273-282 (1993).
- [41] D. Ebert, R. N. Faustov, V. O. Galkin and W. Lucha, Masses of tetraquarks with two heavy quarks in the relativistic quark model, Phys. Rev. D **76**, 114015 (2007).
- [42] W. Park, S. Noh and S. H. Lee, Masses of the doubly heavy tetraquarks in a constituent quark model, Nucl. Phys. A **983**, 1-19 (2019).
- [43] Q. F. Lü, D. Y. Chen and Y. B. Dong, Masses of doubly heavy tetraquarks $T_{QQ'}$ in a relativized quark model, Phys. Rev. D **102**, 034012 (2020).
- [44] E. Braaten, L. P. He and A. Mohapatra, Masses of doubly heavy tetraquarks with error bars, Phys. Rev. D **103**, 016001 (2021).
- [45] Y. Kim, M. Oka and K. Suzuki, Doubly heavy tetraquarks in a chiral-diquark picture, Phys. Rev. D **105**, 074021 (2022).
- [46] Y. Song and D. Jia, Mass spectra of doubly heavy tetraquarks in diquark-antidiquark picture, Commun. Theor. Phys. **75**, 055201 (2023).
- [47] A. Ali, Q. Qin and W. Wang, Discovery potential of stable and near-threshold doubly heavy tetraquarks at the LHC, Phys. Lett. B **785**, 605-609 (2018).
- [48] S. Meinel, M. Pflaumer and M. Wagner, Search for $\bar{b}b\bar{u}s$ and $\bar{b}c\bar{u}d$ tetraquark bound states using lattice QCD, Phys. Rev. D **106**, 034507 (2022).
- [49] C. Alexandrou, J. Finkenrath, T. Leontiou, S. Meinel, M. Pflaumer and M. Wagner, Shallow Bound States and Hints for Broad Resonances with Quark Content $\bar{b}c\bar{u}d$ in $B - \bar{D}$ and $B^* - \bar{D}$ Scattering from Lattice QCD, Phys. Rev. Lett. **132**, 151902 (2024).
- [50] M. Padmanath, A. Radhakrishnan and N. Mathur, Bound Isoscalar Axial-Vector $bc\bar{u}\bar{d}$ Tetraquark T_{bc} from Lattice QCD Using Two-Meson and Diquark-Antidiquark Variational Basis, Phys. Rev. Lett. **132**, 20 (2024).
- [51] A. Radhakrishnan, M. Padmanath and N. Mathur, Study of the isoscalar scalar $bc\bar{u}\bar{d}$ tetraquark T_{bc} with lattice QCD, Phys. Rev. D **110**, 034506 (2024).
- [52] M. Z. Liu and L. S. Geng, Investigations of the weak decays of $D\bar{B}$ molecules, Phys. Rev. D **110**, 053002 (2024).
- [53] R. Machleidt and D. R. Entem, Chiral effective field theory and nuclear forces, Phys. Rept. **503**, 1-75 (2011).
- [54] H. W. Hammer, S. König and U. van Kolck, Nuclear effective field theory: status and perspectives, Rev. Mod. Phys. **92** (2020), 025004.
- [55] H. Xu, B. Wang, Z. W. Liu and X. Liu, DD^* potentials in chiral perturbation theory and possible molecular states, Phys. Rev. D **99**, 014027 (2019) [erratum: Phys. Rev. D **104**, 119903 (2021)].
- [56] B. Wang and L. Meng, Revisiting the DD^* chiral interactions with the local momentum-space regularization up to the third order and the nature of T_{cc}^+ , Phys. Rev. D **107**, 094002 (2023).
- [57] B. Wang, Z. W. Liu and X. Liu, $\bar{B}^{(*)}\bar{B}^{(*)}$ interactions in chiral effective field theory, Phys. Rev. D **99**, 036007 (2019).
- [58] H. Xu, Study of the hidden charm $D\bar{D}^*$ interactions in chiral effective field theory, Phys. Rev. D **105**, 034013 (2022).
- [59] L. Meng, B. Wang, G. J. Wang and S. L. Zhu, The hidden charm pentaquark states and $\Sigma_c\bar{D}^{(*)}$ interaction in chiral perturbation theory, Phys. Rev. D **100**, 014031 (2019).
- [60] B. Wang, L. Meng and S. L. Zhu, Hidden-charm and hidden-bottom molecular pentaquarks in chiral effective field theory, JHEP **11** (2019), 108.
- [61] B. Wang, L. Meng and S. L. Zhu, Molecular tetraquarks and pentaquarks in chiral effective field theory, Nucl. Part. Phys. Proc. **324-329**, 45-48 (2023).
- [62] E. Epelbaum, H. Krebs and U. G. Meißner, Improved chiral nucleon-nucleon potential up to next-to-next-to-next-to-leading order, Eur. Phys. J. A **51**, 53 (2015).
- [63] M. Thomson, Modern particle physics, Cambridge University Press, 2013.
- [64] H. Zhai, Ultracold Atomic Physics, Cambridge University Press, 2021.
- [65] J. R. Taylor, Scattering Theory: The Quantum Theory of Nonrelativistic Collisions, John Wiley & Sons, Inc., 1972.